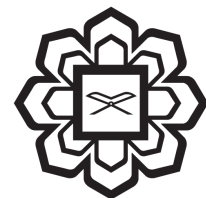


# **DESIGN AND CONTROL OF A SINGLE-LEGGED ROBOT FOR AUTONOMOUS TAKEOFF AND LANDING**

**NIK ADAM MUQRIDZ BIN ABDUL HAKHAM 2125501**

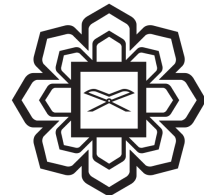


**DEPARTMENT OF MECHANICAL AND AEROSPACE  
ENGINEERING  
KULLIYYAH OF ENGINEERING  
INTERNATIONAL ISLAMIC UNIVERSITY MALAYSIA  
FEBRUARY 2026**

# **DESIGN AND CONTROL OF A SINGLE-LEGGED ROBOT FOR AUTONOMOUS TAKEOFF AND LANDING**

**NIK ADAM MUQRIDZ BIN ABDUL HAKHAM 2125501**

**Project Supervisor: Dr. Hafiz Bin Iman**



**A REPORT SUBMITTED IN PARTIAL FULFILMENT OF THE  
REQUIREMENT FOR A DEGREE OF BACHELOR OF  
AEROSPACE ENGINEERING (HONOURS)**

## **ABSTRACT**

## **ACKNOWLEDGEMENTS**

I extend my deepest gratitude to Almighty Allah for His blessings and guidance throughout this research journey, without which this endeavor would not have been possible. My sincerest appreciation goes to my esteemed supervisor, Dr. Hafiz Bin Iman, for his invaluable guidance, unwavering support, constructive criticism, and profound insights. His expertise and encouragement were instrumental in shaping this project from its inception to completion, providing direction even through the most challenging phases. I am profoundly thankful to the International Islamic University Malaysia (IIUM) and the Department of Mechanical and Aerospace Engineering for providing an exceptional academic environment, state-of-the-art facilities, and the necessary resources that facilitated this research. The knowledge imparted by all my lecturers has laid a strong foundation for this work. I also wish to express my heartfelt thanks to my beloved family, whose constant love, prayers, and emotional support have been my greatest motivation. Their patience and understanding were a continuous source of strength. Finally, I am grateful to my friends and colleagues for their camaraderie, stimulating discussions, and support that enriched my experience throughout this final year project.

## TABLE OF CONTENTS

ABSTRACT.....	7
ACKNOWLEDGEMENTS.....	8
TABLE OF CONTENTS.....	9
LIST OF TABLES.....	11
LIST OF FIGURES.....	12
LIST OF ABBREVIATIONS.....	13
CHAPTER 1 INTRODUCTION.....	1
1.1 BACKGROUND OF STUDY.....	2
1.2 MOTIVATION.....	3
1.3 PROBLEM STATEMENT.....	3
1.4 RESEARCH OBJECTIVES.....	4
1.5 SCOPE OF RESEARCH.....	4
1.6 REPORT ORGANIZATION.....	5
CHAPTER 2 LITERATURE REVIEW.....	6
2.1 SINGLE-LEGGED ROBOT LOCOMOTION.....	7
2.1.1 Hopping Dynamics.....	7
2.1.2 Bio-Inspired Robots.....	9
2.2 LEGGED MAVS LOCOMOTION.....	13
2.2.1 Rotary-Wing Legged MAVs.....	13
2.2.2 Flapping-Wing Legged MAVs.....	15
2.3 CONTROL CHALLENGES.....	18
2.3.1 Dynamic Instability.....	18
2.3.2 The Heavy-Leg Problem: Inertial Coupling.....	19
2.3.3 Quantifying Stability: The Sufficiency Region.....	19
2.4 CONTROL STRATEGIES.....	21
2.4.1 Stance Phase: Trajectory Tracking (Huang & Zhang).....	21
2.4.2 Trajectory Optimization (Yue et al.).....	22
2.4.3 Flight Phase: Angular Momentum Control (Yim et al.).....	23
2.5 RESEARCH GAPS.....	25
2.5.1 Summary of Literature.....	25
2.5.2 Identified Research Gaps.....	26
CHAPTER 3 RESEARCH METHODOLOGY.....	27
3.1 RESEARCH FRAMEWORK.....	28
3.2 SYSTEM MODELING AND DYNAMICS.....	30
3.2.1 Governing Equations of Motion.....	30
3.2.2 Kinematic Analysis.....	32
A. Forward Kinematics (FK).....	32
B. Inverse Kinematics (IK).....	33
C. Jacobian matrix.....	33

3.2.3 Dimensionless Ratios and System Parameters.....	34
3.3 CONTROL ARCHITECTURES.....	36
3.3.1 Finite State Machine (FSM).....	36
3.3.2 Stance Phase: Virtual Model Control (VMC).....	37
3.3.3 Flight Phase: Inertial & Landing Control.....	38
3.3.4 Adaptive Gain Scheduling.....	39
3.4 EXPERIMENTAL VALIDATION.....	39
3.4.1 Disturbance Injection Method.....	40
3.4.2 Stability Search Algorithm.....	41
3.4.4 Summary of Experimental Parameters.....	42
CHAPTER 4 RESULTS AND DISCUSSION.....	43
4.1 PHASE 1: NOMINAL FLIGHT PERFORMANCE.....	44
4.1.1 Kinematic Tracking and Apex Achievement.....	44
4.1 PHASE 1: NOMINAL FLIGHT PERFORMANCE.....	45
4.2.1 Successful Recovery Analysis (Stable Region).....	45
4.2.2 Failure Mode Analysis (Unstable Region).....	46
4.3 STABILITY SUFFICIENCY REGION.....	47
4.3.1 The Stability Map.....	47
4.3.2 Analysis of the Stability Boundary.....	48
4.4 DISCUSSION.....	49
4.4.1 Effectiveness of Adaptive Gain Scheduling.....	49
4.4.2 Design Implications for MAVs.....	49
4.4.3 Summary.....	49
CHAPTER 5 CONCLUSION AND RECOMMENDATIONS.....	50
5.1 CONCLUSION.....	50
5.2 RECOMMENDATION.....	51
REFERENCES.....	52
APPENDIX A RESEARCH GAP METADATA.....	55

## **LIST OF TABLES**

Table 2.1 Comparison of Hopping Dynamics, Bio-inspired Robots, and Research	12
Table 2.2 Comparison of Existing Legged MAV Platforms and Research Directions	17
Table 2.3 Summary of Control Challenges	20
Table 2.4 Comparison of Control Strategies and Proposed Hierarchical Approach.	24
Table 3.1 SLATOL System Parameters for PyBullet Simulation	35
Table 3.2 Finite State Machine Logic and Triggers	36
Table 3.3 Control Parameters and Adaptive Scaling Laws	39
Table 3.4 Experimental Protocol Settings	42
Table 4.1 Stability Limits and Quality Metrics	48

## LIST OF FIGURES

Figure 1.1 Biological Hopping vs. Robotic Hopping (Kovac et al., 2010)	2
Figure 2.1 One-Legged Hopping Kinematic Model (Huang & Zhang, 2023)	8
Figure 2.2 Slip Model Hopping Dynamics (Huang & Zhang, 2023)	8
Figure 2.3 Complete Hopping Sequence (Ugurlu, 2008)	9
Figure 2.4 Birdbot Leg Design Network (Badri-Spröwitz et al., 2022)	10
Figure 2.5 SELDA (Bolignari et al., 2022)	10
Figure 2.6 Salto-1P (Yim et al., 2020) and TTI-Hopper (Ugurlu, 2020)	11
Figure 2.7 SNAG Robot (Roderick et al., 2021)	14
Figure 2.8 SNAG Robot with Different Toe Arrangements (Roderick et al., 2021)	14
Figure 2.9 BOLT MAVs (Roderick et al., 2021)	15
Figure 2.10 P-Flap MAVs (Zufferey et al., 2022)	16
Figure 2.11 Uncertainty at a Touchdown State (Ugurlu, 2008)	18
Figure 2.12 The Perching Sufficiency Region (Roderick et al., 2021)	20
Figure 2.13 Standard SLIP Controller Architecture (Huang & Zhang, 2023)	22
Figure 2.14 NLP Controller Architecture (Yue et al., 2021)	22
Figure 2.15 Salto-1P Reaction Wheel Control Architecture (Yim et al., 2020)	23
Figure 3.1 SLATOL Research Methodology Flowchart	29
Figure 3.2 PyBullet Simulation Environment and URDF Model	31
Figure 3.3 2-Joint Model of SLATOL	32
Figure 3.4 Control Loop Diagram	37
Figure 4.1 Vertical Position ( $z$ ) and Pitch Angle ( $\theta$ ) vs. Time for a Nominal Hop	44
Figure 4.2 Pitch Angle ( $\theta$ ) vs. Time showing Convergence	45
Figure 4.3 Pitch Angle ( $\theta$ ) vs. Time showing Divergence	46
Figure 4.4 Stability Sufficiency Map (Scatter Plot with Boundary Curve)	47

## **LIST OF ABBREVIATIONS**

BLDC	Brushless Direct Current
CAD	Computer-Aided Design
CG	Center of Gravity
CoM	Center of Mass
CoP	Center of Pressure
DOF	Degrees of Freedom
FSM	Finite-State Machine
FYP	Final Year Project
IIUM	International Islamic University Malaysia
IMU	Inertial Measurement Unit
LIP	Linear Inverted Pendulum
MAV	Micro Aerial Vehicle
MPC	Model Predictive Control
NLP	Nonlinear Programming
PID	Proportional-Integral-Derivative
RL	Reinforcement Learning
ROS	Robot Operating System
SBC	Single Board Computer
SLATOL	Single-Legged Autonomous Takeoff and Landing
SLIP	Spring-Loaded Inverted Pendulum
SNAG	Stereotyped Nature-inspired Aerial Grasper
TO	Trajectory Optimization
TOL	Takeoff and Landing
UAV	Unmanned Aerial Vehicle
URDF	Unified Robot Description Format
VMC	Virtual Model Control
ZMP	Zero-Moment-Point

## **CHAPTER 1 INTRODUCTION**

This chapter establishes the foundational framework for the research. Section 1.1 provides the background on avian-inspired robotics and the limitations of current MAVs. Section 1.2 articulates the motivation for developing a hybrid air-ground platform. Section 1.3 defines the specific problem statement regarding dynamic instability. Section 1.4 outlines the research objectives, followed by the scope in Section 1.5. Finally, Section 1.6 details the organization of the report.

## 1.1 BACKGROUND OF STUDY

The field of robotics is increasingly moving towards multimodal mobility to overcome the limitations of single-domain platforms. While fixed-wing and rotary-wing Micro Aerial Vehicles (MAVs) offer exceptional range and agility in open air, they suffer from high energy consumption during hovering and cannot interact physically with the environment. Conversely, terrestrial robots are energy-efficient but limited by complex terrain. Nature offers a solution to this trade-off in the form of avian locomotion; birds utilize their legs not just for perching, but as high-force impulsive launchers to bridge the gap between static ground stability and aerodynamic flight.

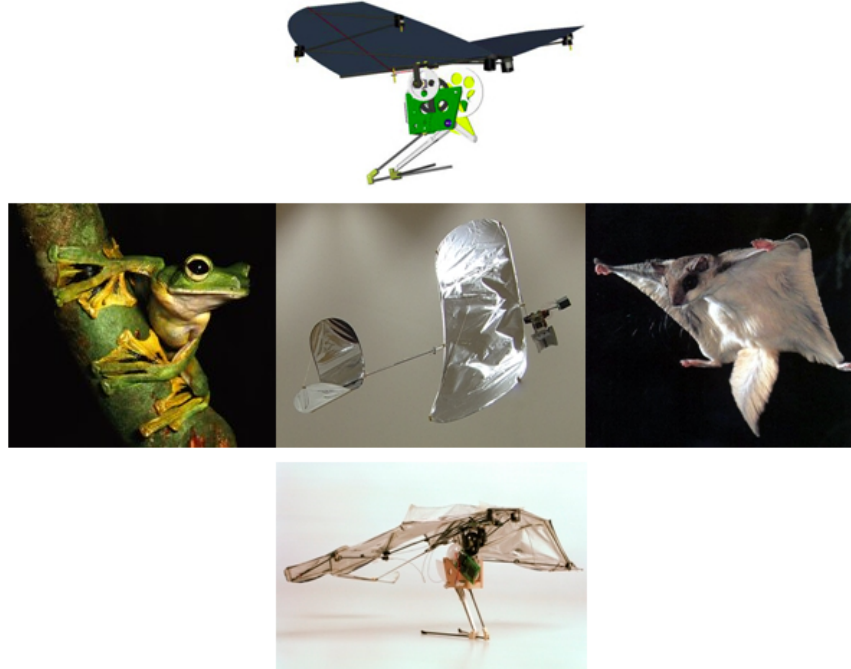


Figure 1.1 Biological Hopping vs. Robotic Hopping (Kovac et al., 2010)

This research focuses on the Single-Legged Autonomous Takeoff and Landing (SLATOL) robot. By integrating a robotic leg with a fixed-wing MAV configuration, the system aims to replicate this biological capability, using the leg to store and release kinetic energy for explosive takeoffs.

## 1.2 MOTIVATION

Agile MAVs capable of perching can perform long-duration environmental monitoring or infrastructure inspection with minimal energy consumption, aligning with sustainable automated maintenance practices. In scenarios such as post-earthquake reconnaissance, ground debris renders wheeled rovers useless, while continuous flight drains MAV batteries rapidly. A hybrid "Jump-Glider" could hop over obstacles, perch on debris to conserve energy, and relaunch instantly. However, realizing this requires a control framework capable of handling the extreme instability of the launch phase—a problem that remains an open challenge in robotics literature.

## 1.3 PROBLEM STATEMENT

Current avian-inspired robots face a critical stability dilemma known as the "Heavy Leg" problem. While biological data shows bird legs constitute 20-30% of body mass (Shin et al., 2024), standard control templates like the SLIP model assume massless legs to simplify dynamics (Huang & Zhang, 2023). This assumption leads to Inertial Coupling, where swinging a heavy leg generates reaction torques that destabilize the robot's pitch in mid-air (Ugurlu, 2021).

Existing solutions fail to bridge the gap between speed and accuracy. Open-loop kinematic controllers are fast but "blind" to these inertial disturbances, causing tumbling. Conversely, optimization-based methods (NLP) are physically accurate but suffer from a Latency Gap, requiring computation times that exceed the short flight phase of a hop (Yue et al., 2021). Consequently, there is no defined "Stability Sufficiency Region" quantifying exactly how heavy a leg can be before its inertial momentum renders the robot uncontrollable under wind stress (Roderick et al., 2021).

## 1.4 RESEARCH OBJECTIVES

The primary aim is to determine the physical stability limits of a single-legged robot by computationally mapping its Stability Sufficiency Region. This will be achieved through the following objectives:

1. To **develop** a high-fidelity dynamic model in PyBullet that explicitly captures the Inertial Coupling effects of variable leg masses (5% to 30% of total mass).
2. To **synthesize** a Hybrid Reactive Controller that integrates virtual spring stance regulation with active angular momentum flight control to reject disturbances in real-time.
3. To **quantify** the operational boundaries by generating a Stability Sufficiency Map, defining the maximum Wind Disturbance the system can withstand across a spectrum of Leg Mass Ratios.

## 1.5 SCOPE OF RESEARCH

1. **Simulation Environment:** Validation is performed exclusively in the PyBullet physics engine. This platform is selected for its high-speed constraint solving, enabling the thousands of iterative simulations required to map the stability region.
2. **Dimensionality:** The analysis is constrained to the 2D sagittal plane. This isolates pitch dynamics and vertical hopping energetics from lateral coupling effects.
3. **Key Variables:** The study focuses strictly on the interaction between Leg Mass Ratio (Morphology) and Lateral Wind Force (Environment). Effects of uneven terrain, aerodynamic lift from wings, and 3D turning maneuvers are excluded.

## **1.6 REPORT ORGANIZATION**

This report is organized as follows: Chapter 1 introduces the heavy-leg instability problem and research motivation. Chapter 2 reviews the literature, highlighting the gaps in existing kinematic and optimization-based controllers. Chapter 3 details the methodology, including the PyBullet system modeling, the hybrid control architecture, and the "Stability Search" experimental protocol. Chapter 4 presents the results, analyzing the generated Stability Sufficiency Maps and failure boundaries. Chapter 5 concludes the research with design guidelines for heavy-legged avian robots.

## **CHAPTER 2 LITERATURE REVIEW**

Chapter 2 will examine the literature relevant to the problem of achieving stable and controlled autonomous takeoff and landing for single-legged robots. It will cover research that supports the project's objectives of designing a dynamically stable platform and developing the required control algorithms. It will include the single-legged robot locomotion (2.1), legged MAV locomotion (2.2), control challenges (2.3), and existing control strategies (2.4). The identified research gaps (2.5) will further motivate the problem statement and objectives of this thesis.

## 2.1 SINGLE-LEGGED ROBOT LOCOMOTION

Single-legged robot locomotion has been a fundamental area of research in legged robotics, serving as a building block for understanding more complex multi-legged systems (Huang & Zhang, 2023). This section explores the dynamics of hopping, the principles behind bio-inspired designs, and the specific challenges introduced by heavy limb morphologies.

### 2.1.1 Hopping Dynamics

Hopping is a fundamental dynamic behavior for legged robots and a precursor to running. The dynamics of hopping are highly nonlinear and non-smooth due to interactions with the environment. To ensure stability during jumping, this study utilizes discretized Zero-Moment-Point (ZMP) equations in polar coordinates to include angular momentum smoothly (Ugurlu, 2008).

A common model used to simplify and understand the mechanics of hopping and running is the Spring-Loaded Inverted Pendulum (SLIP) model. The SLIP model represents the robot as a point mass on a massless leg with a linear spring. Huang and Zhang (2023) employed the SLIP model to control the jumping of a one-legged robot and map jumping height to foot force, mimicking animal jumping control mechanisms as visualized in **Figure 2.1** and **Figure 2.2**.

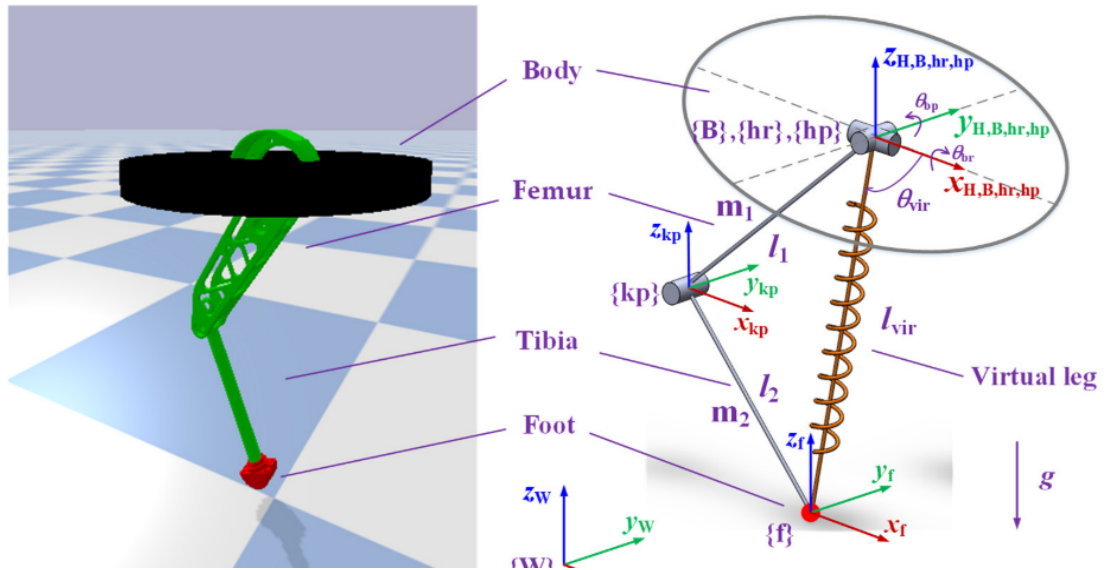


Figure 2.1 One-Legged Hopping Kinematic Model (Huang & Zhang, 2023)

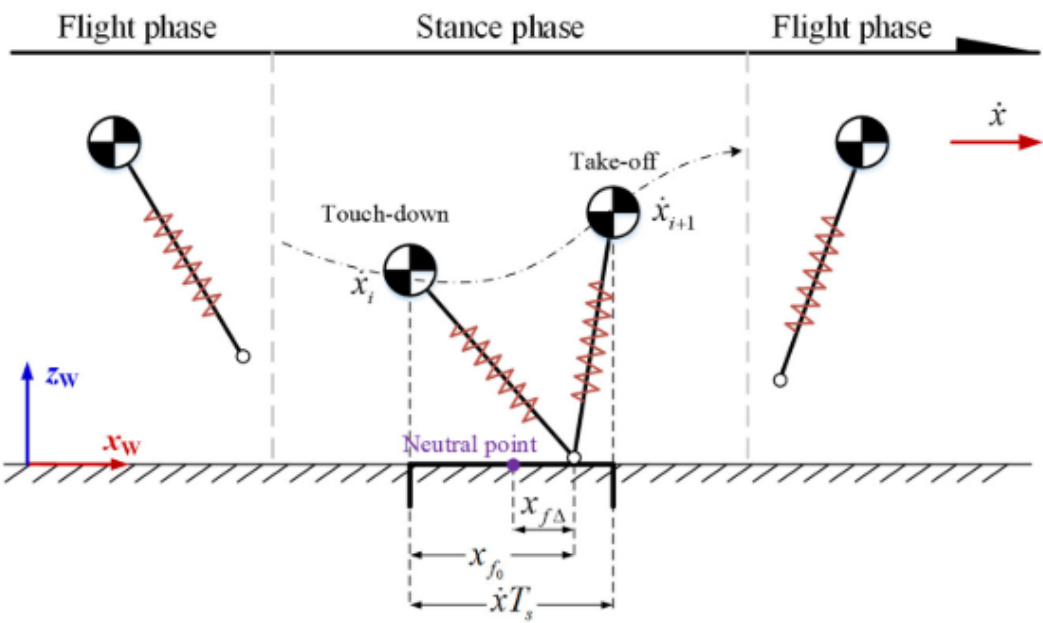


Figure 2.2 Slip Model Hopping Dynamics (Huang & Zhang, 2023)

The hopping process can be decomposed into distinct phases, typically stance (foot on ground) and flight (foot off ground), which are further divided into sub-phases like compression, thrust, swing, and landing. Switching between the stance and flight phases is critical for maintaining continuous locomotion. Accurately generating real-time jumping patterns that ensure overall stability through a complete jumping cycle, as shown in **Figure 2.3**, is essential for system robustness (Ugurlu, 2008).

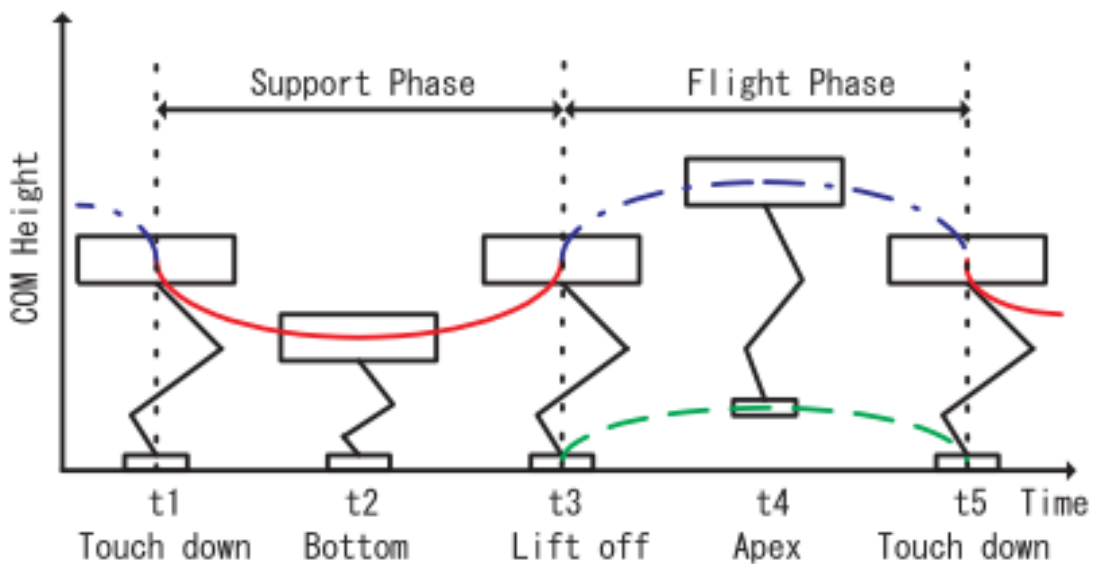


Figure 2.3 Complete Hopping Sequence (Ugurlu, 2008)

### 2.1.2 Bio-Inspired Robots

Drawing inspiration from biological systems has been a successful approach in designing agile and efficient legged robots. Avian locomotion, in particular, provides valuable insights for monopodal design. For instance, BirdBot uses a spring tendon network and a bistable joint reminiscent of self-engaging clutches observed in large birds like ostriches (Badri-Spröwitz et al., 2022), as shown in **Figure 2.4**.

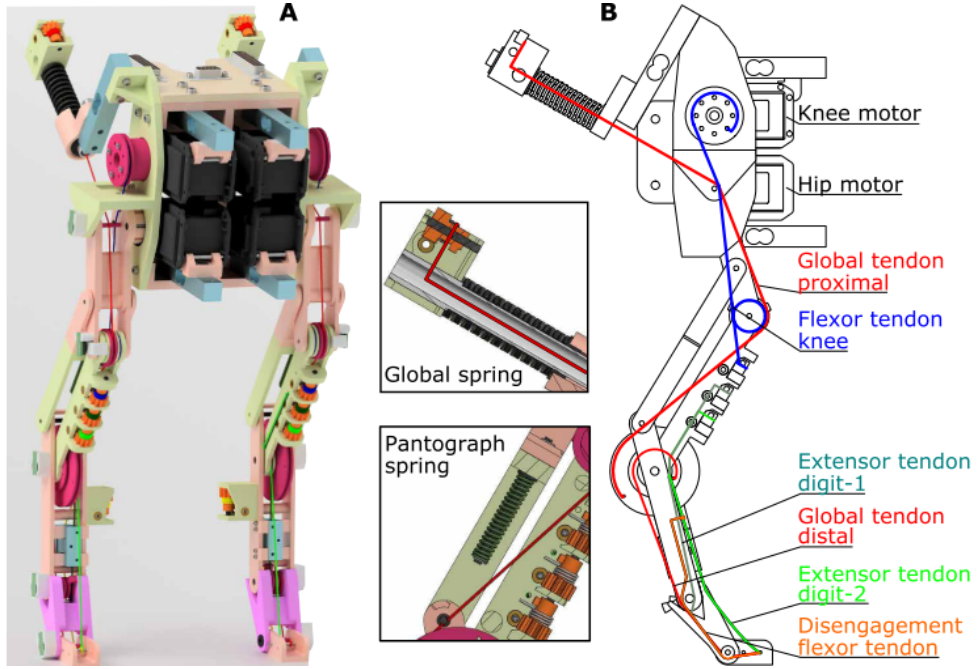


Figure 2.4 Birdbot Leg Design Network (Badri-Spröwitz et al., 2022)

Another approach involves integrating compliance into muscle-tendon units for energy-efficient locomotion. The Series ELastic Diaphragm for distal Actuation (SELD) shown in **Figure 2.5** was developed to provide lightweight, low-inertia, and compliant distal actuation for agile hopping (Bolignari et al., 2022).

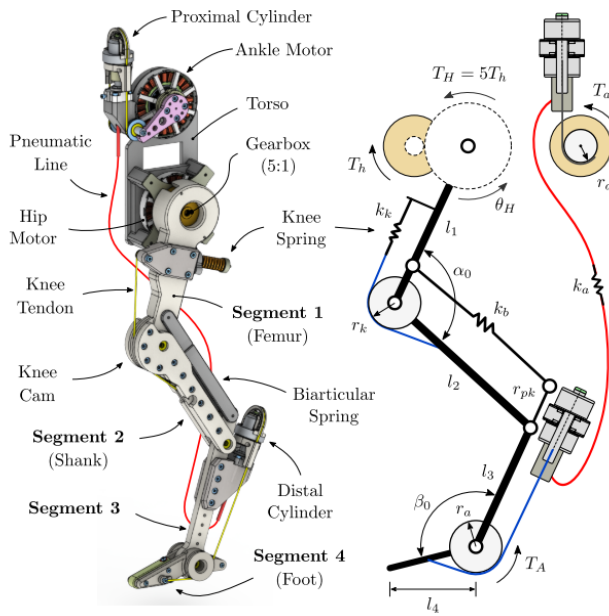


Figure 2.5 SELDA (Bolignari et al., 2022)

Robots like Salto-1P and TTI-Hopper in **Figure 2.6** are examples of monopedal bio-inspired platforms used to investigate dynamic behaviors like hopping and balancing. Salto-1P, with a body length of 0.313m, uses onboard sensors for state estimation during high-acceleration hopping. TTI-Hopper is an untethered 4-link, 3-DOF one-legged robot designed to study running dynamics. These platforms are typically actuated by Brushless DC (BLDC) motors, which are selected for their high power density and efficiency—critical factors for achieving the rapid acceleration and high-torque maneuvers required in monopedal systems. These robots leverage compliant designs and control strategies, such as admittance control, to handle contact forces and achieve stable running locomotion.

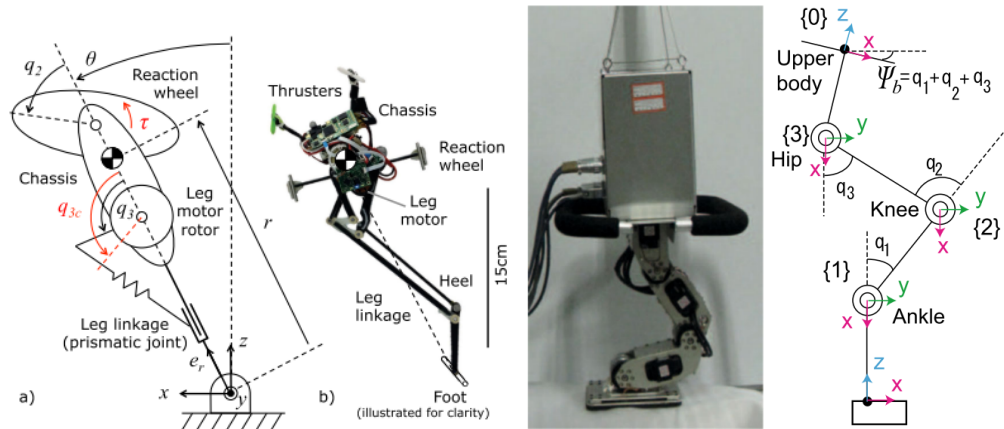


Figure 2.6 Salto-1P (Yim et al., 2020) and TTI-Hopper (Ugurlu, 2020)

Table 2.1 Comparison of Hopping Dynamics, Bio-inspired Robots, and Research

Feature	Hopping Dynamics (SLIP/ZMP)	Bio-inspired Robots (Salto/BirdBot)	Proposed Approach (This Research)
<b>Past Work Examples</b>	Huang & Zhang (2023); Ugurlu (2008)	Yim et al. (2020); Roderick et al. (2021)	Integrated SLATOL Framework
<b>Focus</b>	Fundamental stability and trajectory planning.	Mechanical efficiency and real-world agility.	Runway-independent launch and landing stability.
<b>Actuation</b>	Idealized force/torque inputs.	Compliant actuators / Tendon networks.	<b>High-power density BLDC motors</b> for impulsive launch.
<b>Complexity</b>	Simplified (Point mass/Linear spring).	High (Multi-link/ Non-linear tendons).	<b>Balanced (2-axis/2-DOF)</b> kinematic model.
<b>Environment</b>	Limited to planar/ideal simulations.	High sensorimotor noise and impact forces.	<b>PyBullet</b> with planar constraints.
<b>Limitation</b>	Lacks environmental noise modeling.	High power requirements and weight trade-offs.	Isolated ground-to-air transition dynamics.

As shown in **Table 2.1**, while theoretical models like the SLIP provide a reliable baseline for stability, they often overlook the practical limitations of physical actuators. Conversely, complex bio-inspired robots like Salto-1P demonstrate extreme agility but require significant computational overhead. This research seeks to bridge these domains by utilizing the computational efficiency of the SLIP model for high-level trajectory planning, while employing high-torque BLDC motors to provide the impulsive force necessary for a fixed-wing MAV takeoff. By focusing on a 2-axis configuration, the study isolates the core modeling problem of integrating impulsive launching with aerodynamic lift.

## 2.2 LEGGED MAVS LOCOMOTION

While legged robots navigate terrestrial environments, Micro Aerial Vehicles (MAVs)—a classification of smaller Unmanned Aerial Vehicles (UAVs) typically weighing less than 1 kg—operate in the air. Combining these capabilities into a single system presents unique opportunities for locomotion in complex, arboreal, or uneven 3D environments. Currently, the most well-known types of legged MAVs are rotary-wing and flapping-wing platforms.

### 2.2.1 Rotary-Wing Legged MAVs

The integration of legs onto MAVs allows for hybrid locomotion strategies, enabling tasks like perching, grasping, and potentially more stable landing on challenging surfaces where purely aerial approaches are difficult or impossible. Bird-inspired designs have been particularly influential in this domain, focusing on mechanisms for dynamic grasping and perching in arboreal environments.

The SNAG robot (Stereotyped Nature-inspired Aerial Grasper), shown in **Figure 2.7**, is a prime example, featuring bird-inspired legs and grasping mechanisms designed for perching on branches. SNAG's leg design includes analogs of avian muscle-tendon structures and utilizes a quick-release mechanism to rapidly deploy grasp force upon impact. As visualized in **Figure 2.8**, achieving successful perching depends on various factors, including toe arrangement (anisodactyl vs. zygodactyl), trigger timing, and impact velocity.

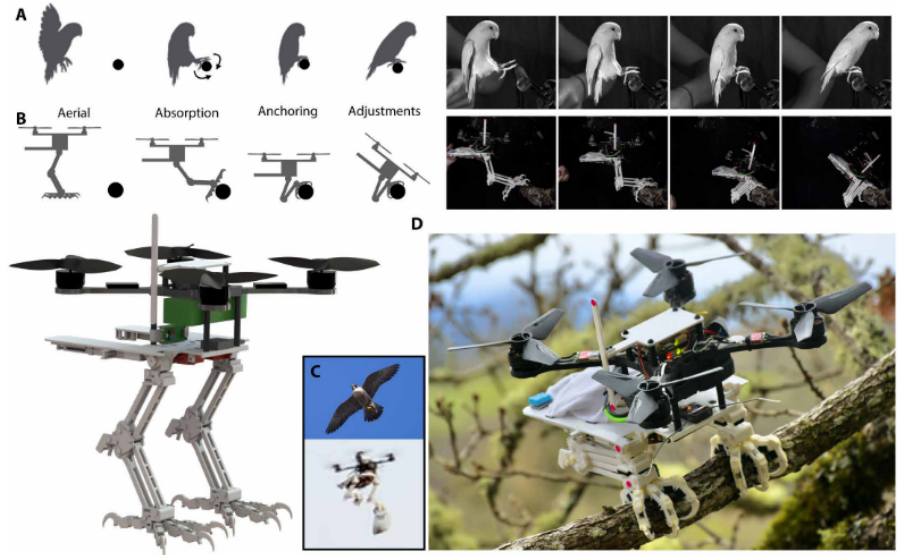


Figure 2.7 SNAG Robot (Roderick et al., 2021)

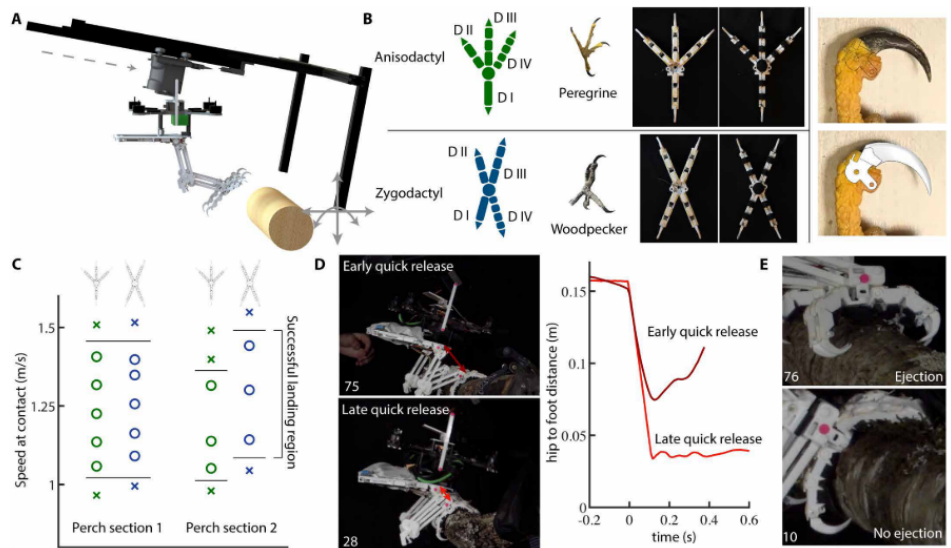


Figure 2.8 SNAG Robot with Different Toe Arrangements (Roderick et al., 2021)

## 2.2.2 Flapping-Wing Legged MAVs

While many legged MAVs are quadrotors, the concept extends to fixed-wing or flapping-wing (ornithopter) platforms. The BOLT robot is an example of a system designed for both terrestrial and aerial locomotion, combining the gearbox and wings from a commercial ornithopter with custom legs. A single motor drives both the legs and wings, highlighting the challenge of achieving sufficient power density for flight while also enabling terrestrial movement. BOLT, as shown in **Figure 2.9**, utilizes flapping wings and a tail to maintain passive stability when running, demonstrating a truly bipedal gait at higher speeds.

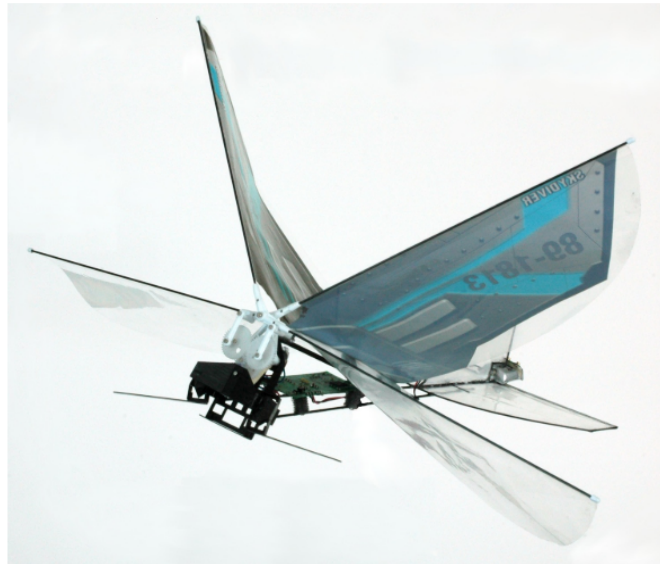


Figure 2.9 BOLT MAVs (Roderick et al., 2021)

Another flapping-wing robot, P-Flap in **Figure 2.10**, has been adapted for perching experiments, focusing on autonomous perching on a branch. The leg mechanism for perching is active and designed to compensate for flight inaccuracies, change the robot's pose after perching for stability, and maintain equilibrium. Key constraints include size, weight, impact resistance, and the speed/power of actuation.

The control strategy for flapping-wing perching involves controlling pitch, yaw, and height, often tuned around a specific feasible trajectory due to the highly nonlinear flight dynamics. Perching flight requires reducing forward velocity upon approaching the target. Future work includes enabling the robot to take off from the branch, requiring strategies like posture correction, utilizing friction for slow claw release, executing a forward jump, or even a controlled fall followed by flight recovery (Zufferey et al., 2022).

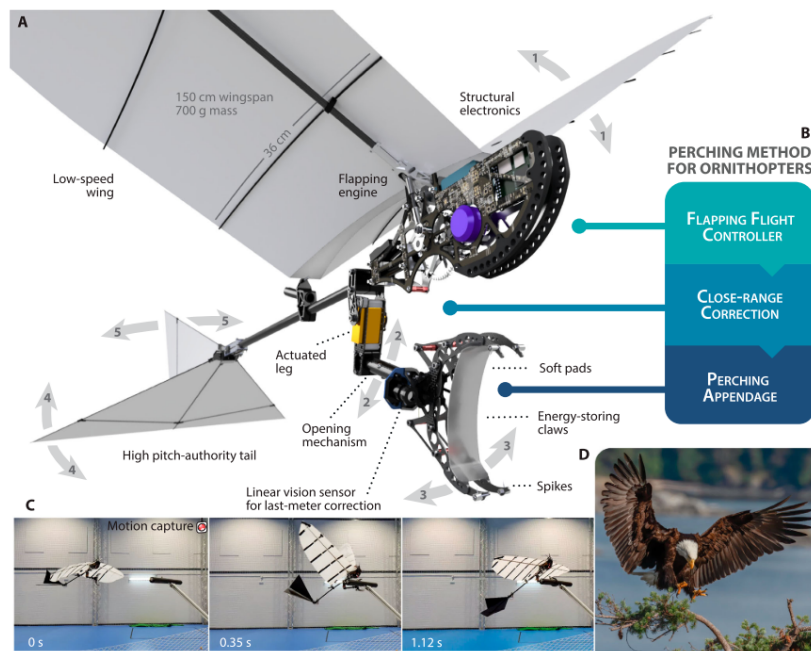


Figure 2.10 P-Flap MAVs (Zufferey et al., 2022)

Table 2.2 Comparison of Existing Legged MAV Platforms and Research Directions

Feature	Rotary-Wing (SNAG)	Flapping-Wing (BOLT/P-Flap)	Proposed Research
<b>Locomotion Type</b>	Multi-rotor flight + Perching	Flapping flight + Running/Perching	<b>Fixed-wing flight + Monopedal launch</b>
<b>Mechanical Goal</b>	Dynamic grasping/climbing	Passive running stability	<b>Runway-independent takeoff</b>
<b>Primary Actuation</b>	Specialized perching motors	Single motor for wings and legs	<b>High-power BLDC impulsive leg</b>
<b>Stability Strategy</b>	Post-impact posture adjustment	Tail-assisted passive balance	<b>SLIP-based active trajectory control</b>
<b>Terrain Focus</b>	Arboreal/Branches	General unstructured terrain	<b>Flat surfaces for ground-to-air transition</b>

As summarized in **Table 2.2**, while rotary and flapping-wing systems have made strides in perching, a fixed-wing MAV utilizing a single leg for autonomous takeoff is relatively unexplored. Unlike traditional fixed-wing aircraft that require runways, the proposed work addresses the inherent dynamic instability of monopedal systems during high-speed transitions.

## 2.3 CONTROL CHALLENGES

Controlling dynamic legged locomotion, especially when combined with aerial phases such as takeoff and landing, presents significant technical hurdles. These challenges stem from the inherent instability of single-legged systems and the precise requirements for transitioning between different locomotive states.

### 2.3.1 Dynamic Instability

Legged locomotion is inherently complex and subject to dynamic instability due to discrete contact events, environmental variations, and sensorimotor noise. Maintaining stability requires robust control of leg-substrate interaction forces, as external perturbations can occur faster than typical control loops can respond. Passive mechanical walkers, while energy-efficient, are particularly sensitive to initial conditions. As noted by Ugurlu (2008), even minor perturbations during the stance phase can lead to catastrophic tumbling during flight if not corrected. This uncertainty at the touchdown state is illustrated in **Figure 2.11**, where the system state becomes unpredictable after impact

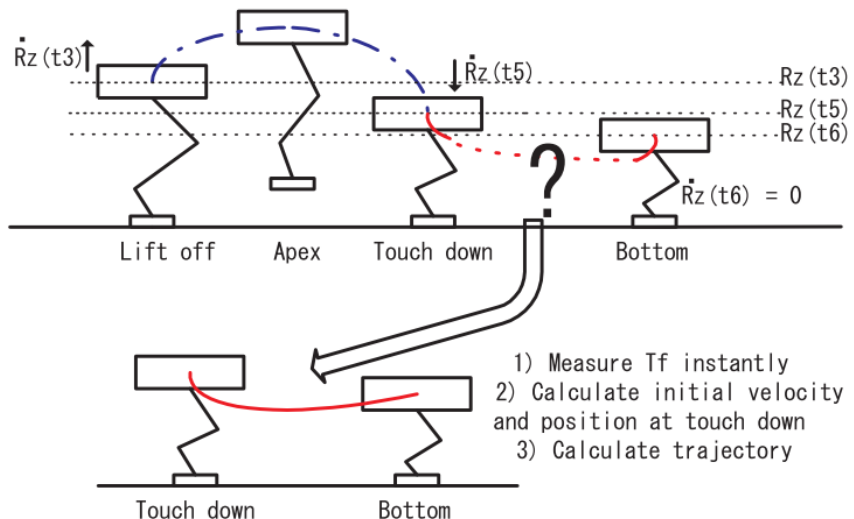


Figure 2.11 Uncertainty at a Touchdown State (Ugurlu, 2008)

### 2.3.2 The Heavy-Leg Problem: Inertial Coupling

A specific challenge for avian-scale robots is the mass of the legs. While standard models like the Spring-Loaded Inverted Pendulum (SLIP) assume massless legs to simplify dynamics, biological legs are heavy, often constituting 20-30% of total body mass (Shin et al., 2024). Ugurlu (2021) mathematically demonstrated that when a leg has significant mass, its motion is governed by the conservation of angular momentum, leading to "Inertial Coupling":

$$I_{body} \ddot{\theta}_{body} \approx - I_{leg} \ddot{\theta}_{leg} \quad (\text{Eq. 2.1})$$

According to Equation 2.1, accelerating a heavy leg forward to prepare for landing generates a reaction torque that forces the body to pitch backward. This interaction creates a specific control challenge: swinging the leg inevitably destabilizes the body pitch, requiring a controller that can actively manage this angular momentum transfer.

### 2.3.3 Quantifying Stability: The Sufficiency Region

Defining "success" in these dynamic maneuvers is difficult because stability is not a simple binary state (Stable/Unstable). Roderick et al. (2021) introduced the concept of the "Stability Sufficiency Region" to evaluate perching performance. Instead of testing a single condition, they mapped a 2D region defined by landing velocity and leg angle, as shown in **Figure 2.12**. The boundary of this region represents the physical limit where the robot's momentum overwhelms its grasping strength or actuator authority. This metric is essential for quantifying the trade-off between morphological properties (e.g., Leg Mass Ratio) and environmental disturbances (e.g., Wind).

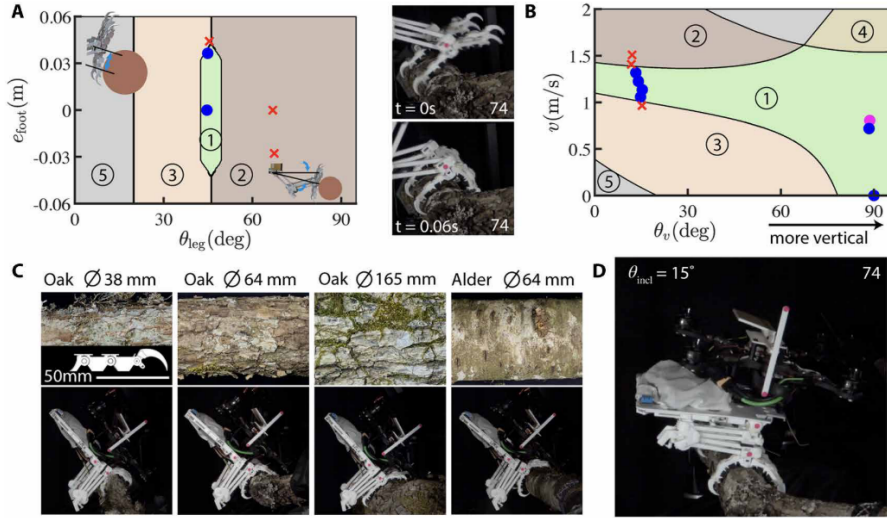


Figure 2.12 The Perching Sufficiency Region (Roderick et al., 2021)

The primary control challenge for the SLATOL robot is maintaining stability during the under-actuated flight phase where external ground forces cannot be applied. The presence of heavy legs introduces inertial coupling, which standard SLIP models ignore. Consequently, a controller must be designed to explicitly manage internal angular momentum to prevent tumbling. A summary of these primary challenges is provided in **Table 2.3**.

Table 2.3 Summary of Control Challenges

Physical Phenomenon	Control Consequence	Failure Mode if Unaddressed
<b>Inertial Coupling (Heavy Legs)</b>	Leg swing creates unwanted body pitch torque	Backward Tumbling during flight or upon landing.
<b>Under-Actuation (Flight Phase)</b>	No ground reaction force is available to correct posture.	Drift; Robot cannot reject wind disturbances while airborne.
<b>Contact Uncertainty (Impact)</b>	Sensor noise makes exact touchdown timing unpredictable.	Knee Collapse; Actuators trigger too early or too late.

## 2.4 CONTROL STRATEGIES

To manage the complex dynamics of heavy-legged hopping, existing research generally falls into three paradigms: Open-Loop Trajectory Tracking, Nonlinear Optimization, and Reactive Momentum Control. This research synthesizes the efficiency of tracking with the robustness of reactive control, while avoiding the computational latency of optimization.

### 2.4.1 Stance Phase: Trajectory Tracking (Huang & Zhang)

The classical approach, formalized by Raibert (1986) and recently applied by Huang & Zhang (2023) to a single-legged robot, decomposes control into three independent parts: hopping height, forward speed, and attitude shown in **Figure 2.13**.

To maintain vertical energy, the controller calculates a virtual spring force during the stance phase. This mimics the Spring-Loaded Inverted Pendulum (SLIP) dynamics:

$$F_{vir} = k_{ss}(l_{vir}^d - l_{vir}) + k_{ds}\dot{l}_{vir} \quad (\text{Eq. 2.2})$$

Where  $k_{ss}$  and  $k_{ds}$  are the stiffness and damping gains.

To maintain a desired forward speed the foot placement relative to the hip is governed by the error in velocity, :

$$x_{land} = \frac{\dot{x}_s^T}{2} + K_{raibert}(\dot{x} - \dot{x}_{des}) \quad (\text{Eq. 2.3})$$

Limitation: While effective on flat ground, Huang's method is "blind" to body pitch during the flight phase. It assumes the body remains upright, which fails when the Inertial Coupling of a heavy leg induces tumbling (as defined in **Eq. 2.1**).

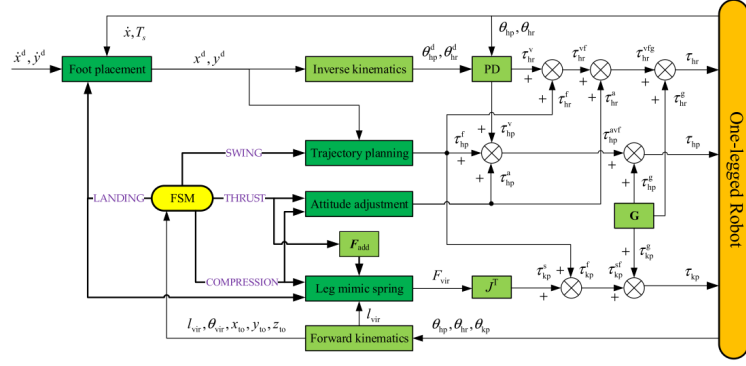


Figure 2.13 Standard SLIP Controller Architecture (Huang & Zhang, 2023)

### 2.4.2 Trajectory Optimization (Yue et al.)

A theoretically optimal approach is Nonlinear Programming (NLP). Yue et al. (2021) shown in **Figure 2.14** applied this to a single-legged vertical hopper, using the IPOPT solver to generate optimal control trajectories ( $u$ ) that adapt to varying workloads.

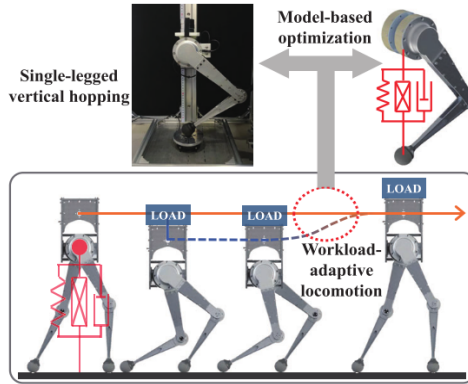


Figure 2.14 NLP Controller Architecture (Yue et al., 2021)

Limitation: While accurate, Yue et al. reported that generating these optimal trajectories can take "seconds" to finish. In the context of this research, where the flight phase lasts less than 300ms, a solver latency of seconds is unacceptable for reacting to sudden wind gusts. Therefore, this study excludes NLP in favor of faster reactive heuristics.

### 2.4.3 Flight Phase: Angular Momentum Control (Yim et al.)

To actively stabilize the body during flight, advanced controllers employ Angular Momentum Control (AMC). Yim et al. (2020) demonstrated this on the Salto-1P robot using a reaction wheel. By accelerating the wheel (or limb) in the air, the robot generates a counter-torque to nullify pitch errors according to the control law:

$$\tau_{control} = -k_p \theta_{body} - k_d \dot{\theta}_{body} \quad (\text{Eq. 2.3})$$

Although Yim used a reaction wheel, as shown in **Figure 2.15**, the mathematical principle applies equally to swinging a heavy leg. This suggests that a robot could stabilize a heavy-legged robot by using the leg itself as a reaction mass, effectively turning the "Heavy Leg" liability into a control asset.

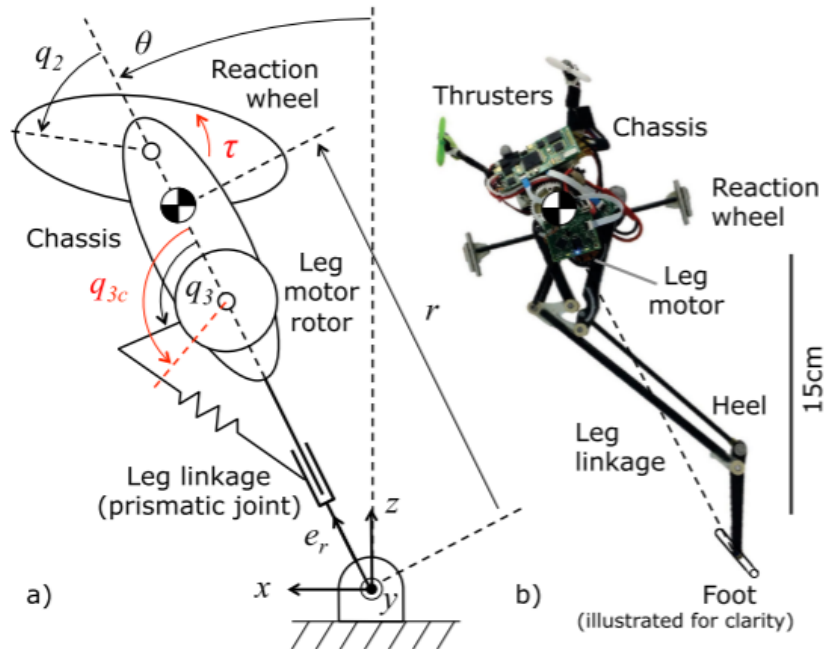


Figure 2.15 Salto-1P Reaction Wheel Control Architecture (Yim et al., 2020)

The literature suggests that Huang's open-loop tracking is insufficient for disturbances, while Yue's NLP optimization is too slow for real-time reaction. The proposed solution must synthesize Huang's energetic efficiency during stance (Eq 2.2, 2.3) with Yim's inertial authority during flight (Eq 2.4) to define the maximum stable Sufficiency Region. A comparison of these strategies is provided in **Table 2.4**.

Table 2.4 Comparison of Control Strategies and Proposed Hierarchical Approach.

Feature	Trajectory Tracking (Huang & Zhang, 2023)	Optimization / NLP (Yue et al., 2021)	Reactive Momentum (Yim et al., 2020)	Proposed Synthesis (This Study)
<b>Primary Method</b>	Pre-planned Kinematics (Bézier Curves)	Numerical Solver (IPOPT)	Inertial Counter-Torque	SLIP (Stance) + AMC (Flight)
<b>Flight Stability</b>	None (Assumes upright)	Perfect (Pre-calculated)	Active (Feedback)	Active (Uses Leg Inertia)
<b>Computation Time</b>	Very Low (Real-time)	High (Seconds)	Low (Real-time)	Low (Real-time)
<b>Robustness</b>	Fails under wind/impact	Fails if model differs	High disturbance rejection	High disturbance rejection
<b>Role in Research</b>	Baseline Control	Excluded (Too slow)	Flight Stabilizer	The Experimental Control

## **2.5 RESEARCH GAPS**

### **2.5.1 Summary of Literature**

Current research in legged locomotion bifurcates into two opposing methodologies. Heuristic approaches, such as Huang & Zhang (2023), prioritize computational speed by using simplified SLIP templates that assume massless legs. Conversely, optimization-based methods like Yue et al. (2021) solve full-body dynamics for high physical fidelity but require excessive computation time. Biological observations by Shin et al. (2024) indicate that avian agility relies on heavy, multifunctional legs (20–30% of body mass), a morphological feature that current "blind" heuristic models fail to stabilize and optimization models fail to control in real-time.

## 2.5.2 Identified Research Gaps

Despite significant progress, three critical gaps prevent robots from replicating avian takeoff and landing agility:

1. **The Inertial Coupling Gap:** Standard kinematic controllers (Huang & Zhang, 2023) ignore the reaction torques generated by swinging heavy legs. Ugurlu (2021) demonstrated that this Inertial Coupling causes catastrophic pitch instability during the flight phase if not actively compensated.
2. **The Latency Gap in Optimization:** Nonlinear Programming (NLP) solvers can theoretically resolve inertial coupling but require computation times on the order of seconds (Yue et al., 2021). This exceeds the typical  $<300\text{ms}$  flight phase of a hop, rendering NLP too slow to reject sudden wind gusts.
3. **Unmapped Stability Sufficiency Region:** While Roderick et al. (2021) defined a "Stability Sufficiency Region" for perching, this metric has not been applied to heavy-legged hopping. The specific physical trade-off between Leg Mass Ratio and Wind Tolerance remains unquantified, leaving no design guidelines for the maximum leg mass a robot can stabilize against wind.

Consequently, this study aims to fill these gaps by computationally mapping the "Stability Sufficiency Region" of a single-legged robot. Instead of comparing controllers, this research will stress-test an integrated control framework (synthesizing Yim's angular momentum control) to rigorously define the operational envelope where heavy-legged locomotion remains viable against wind and inertial disturbances.

## CHAPTER 3 RESEARCH METHODOLOGY

This chapter details the computational framework employed to determine the physical stability limits of the SLATOL robot. Unlike prior studies that utilized fixed morphological parameters, this research adopted a dynamic variable-injection approach within the PyBullet physics engine to map the Stability Sufficiency Region. The methodology is organized as follows: Section 3.1 outlines the research framework and simulation environment. Section 3.2 describes the system modeling, including the derivation of governing equations and the dimensionless ratios used as independent variables. Section 3.3 details the control architecture, focusing on the hybrid state machine and the adaptive gain scheduling algorithm. Finally, Section 3.4 establishes the experimental protocol for the stability search and data analysis.

### 3.1 RESEARCH FRAMEWORK

The research utilized a Model-Based Design (MBD) workflow centered on the PyBullet simulation environment. PyBullet was selected over conventional block-based solvers due to its superior computational efficiency in handling discrete contact events and its direct integration with Python, which facilitated the rapid parameter sweeping required for this study (Huang & Zhang, 2023). The simulation operated at a physics frequency of 1000 Hz to accurately capture high-frequency impact dynamics. The robot was modeled as a floating-base articulated system constrained to the sagittal plane (x–z), allowing for the isolation of pitch dynamics and vertical hopping energetics without the noise of lateral singularities.

As illustrated in **Figure 3.1**, the framework proceeded sequentially through three phases, each directly addressing a specific research objective:

1. **System Modeling (Objective 1):** The physical plant kinematics and dynamics were defined in a URDF format to explicitly capture inertial coupling effects.
2. **Control Synthesis (Objective 2):** A hybrid controller was developed with an adaptive gain scheduling module to compensate for variable leg masses in real-time.
3. **Stability Search (Objective 3):** An iterative experimental loop was executed where the robot's morphology (mass ratio) and environmental conditions (wind force) were progressively degraded to quantify the operational boundaries.

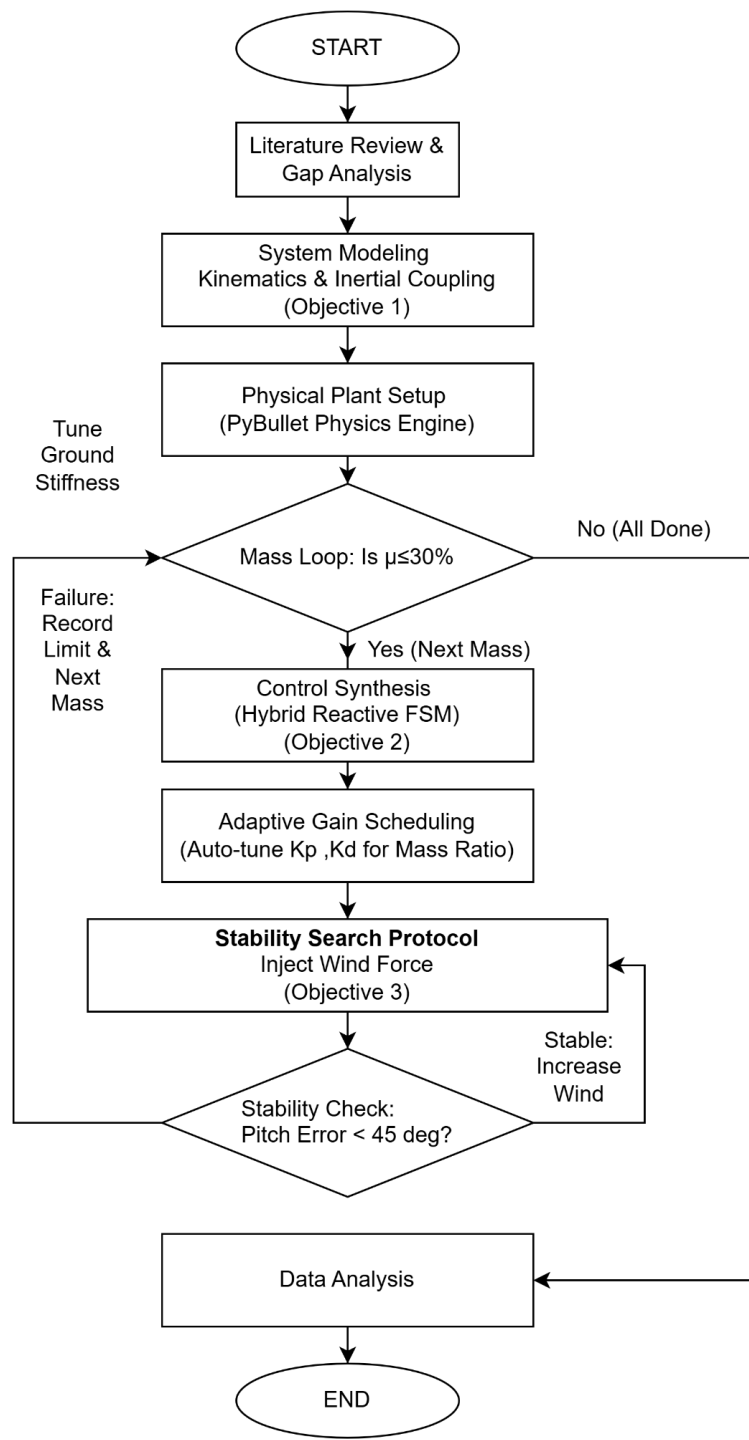


Figure 3.1 SLATOL Research Methodology Flowchart

## 3.2 SYSTEM MODELING AND DYNAMICS

To rigorously evaluate the stability of the SLATOL robot, the system was modeled as a floating-base articulated rigid body within the PyBullet physics engine. Unlike simplified point-mass templates used in previous open-loop studies, this high-fidelity model explicitly captures the non-linear Inertial Coupling effects generated by the heavy leg segments during high-speed aerial maneuvers.

### 3.2.1 Governing Equations of Motion

The motion of the robot is governed by the standard dynamics for floating-base articulated systems. This mathematical formulation explicitly couples the leg's movement to the body's rotation, defined as:

$$M(q) \ddot{q} + C(q, \dot{q}) \dot{q} + G(q) = S^T \tau + J^T F_{ext} \quad (\text{Eq 3.1})$$

- $q$ : The vector of generalized coordinates  $[x, z, \theta_{body}, \theta_{hip}, \theta_{knee}]^T$
- $M(q)$ : The system mass matrix. This matrix is state-dependent, meaning the system's moment of inertia changes as the heavy leg extends or retracts
- $C(q, \dot{q})$ : The Coriolis and centrifugal force vector, significant in rapid leg swings.
- $G$ : The gravitational force vector.
- $\tau, F_{ext}$ : The active joint torques and external forces.

The resulting multibody configuration within the PyBullet environment is visualized in **Figure 3.2**. The simulation was stepped at a physics frequency of 1000 Hz to accurately resolve the discrete contact events during touchdown and takeoff

Figure 3.2 PyBullet Simulation Environment and URDF Model

### 3.2.2 Kinematic Analysis

The control architecture operates in two distinct domains: the Joint Space ( $\theta_1, \theta_2$ ) for actuator commands, and the Virtual Space ( $r, \phi$ ) for the high-level SLIP template. To bridge this domain gap, Forward Kinematics (FK) and Jacobian mappings were derived.

#### A. Forward Kinematics (FK)

The position of the foot relative to the hip coordinate frame ( $x_f, z_f$ ) based on the link lengths  $L_1$  (Femur) and  $L_2$  (Tibia) shown in **Figure 3.3**:

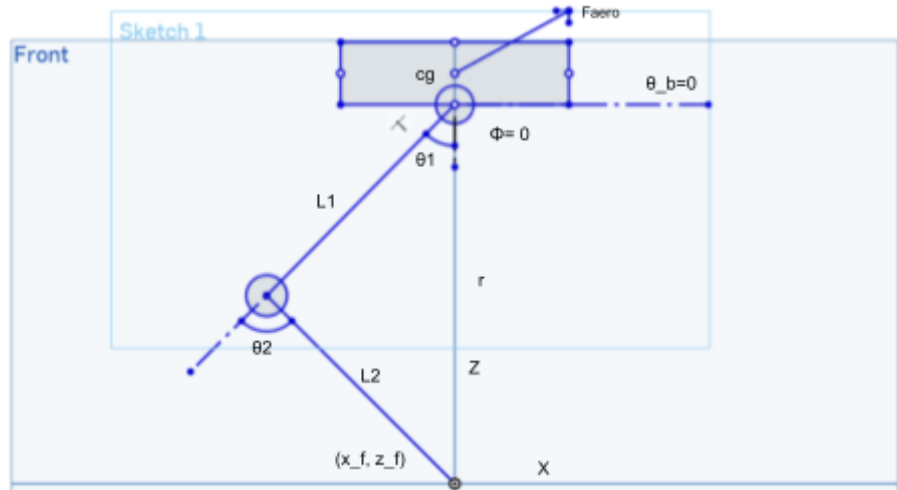


Figure 3.3 2-Joint Model of SLATOL

Foot Position relative to Hip:

$$\begin{aligned} x_{foot} &= L_1 \sin(\theta_1) + L_2 \sin(\theta_1 + \theta_2) \\ z_{foot} &= -L_1 \cos(\theta_1) - L_2 \cos(\theta_1 + \theta_2) \end{aligned} \quad (\text{Eq 3.2})$$

Virtual Coordinates:

$$\begin{aligned} r &= \sqrt{x_f^2 + z_f^2} \\ \phi &= \arctan 2(x_f, -z_f) \end{aligned} \quad (\text{Eq 3.3})$$

## B. Inverse Kinematics (IK)

To execute the Foot Placement strategy, the controller must compute the required joint angles for a desired landing target. Using the Law of Cosines:

$$\begin{aligned}\theta_1 &= \arctan 2(x_{des} - z_{des}) - \arcsin\left(\frac{L_2 \sin(\theta_2)}{\sqrt{x_{des}^2 + z_{des}^2}}\right) \\ \theta_2 &= -\arccos\left(\frac{x_{des}^2 + z_{des}^2 - L_1^2 - L_2^2}{2L_1 L_2}\right)\end{aligned}\quad (\text{Eq 3.4})$$

## C. Jacobian matrix

To implement the virtual spring compliance, the controller calculates a desired force vector in polar coordinates  $(F_r, \tau_\phi)$ . The analytical Jacobian is utilized to map these virtual forces into realizable joint torques  $(\tau_1, \tau_2)$  via the transpose relationship

$$\begin{aligned}\tau_{joints} &= J^T F \\ \begin{bmatrix} \tau_{hip} \\ \tau_{knee} \end{bmatrix} &= \underbrace{\begin{bmatrix} (L_1 c_1 + L_2 c_{12}) & (L_1 s_1 + L_2 s_{12}) \\ L_2 c_{12} & L_2 s_{12} \end{bmatrix}}_{J_{Cartesian}^T} \begin{bmatrix} F_x \\ F_z \end{bmatrix}\end{aligned}\quad (\text{Eq 3.5})$$

Where  $c_1, s_1$  denote  $\cos(\theta_{\text{hip}})$ ,  $\sin(\theta_{\text{hip}})$  and  $c_{12}, s_{12}$  denote  $\cos(\theta_{\text{hip}} + \theta_{\text{knee}})$ ,  $\sin(\theta_{\text{hip}} + \theta_{\text{knee}})$ .

### 3.2.3 Dimensionless Ratios and System Parameters

To quantify the stability boundaries generally, two dimensionless ratios were derived to normalize the robot's morphology against environmental stress.

- **Leg Mass Ratio ( $\mu$ ) :** The primary morphological independent variable is the Leg Mass Ratio ( $\mu$ ). This ratio dictates the magnitude of the angular momentum transfer during the flight phase and serves as the x-axis for the Stability Sufficiency Map

$$\mu = \frac{m_{leg}}{m_{leg} + m_{body}} \quad (\text{Eq 3.6})$$

- **Wind Disturbance Ratio ( $\eta$ ):** To compare stability across different robot weights, the environmental disturbance is normalized as the Wind Disturbance Ratio ( $\eta$ ), defined as the lateral wind force ( $F_{wind}$ ) divided by the robot's total gravitational weight.

$$\eta = \frac{F_{wind}}{m_{total} g} \quad (\text{Eq 3.7})$$

The fixed geometric parameters and variable inertial properties used for the simulation are summarized in **Table 3.1**. The link lengths ( $L_1, L_2$ ) were fixed based on the biological proportions of avian legs capable of agile ground-to-air transition, while the total mass was set to 1.0 kg to comply with the standard classification of Micro Aerial Vehicles (MAVs).

Table 3.1 SLATOL System Parameters for PyBullet Simulation

<b>Component</b>	<b>Parameter</b>	<b>Symbol</b>	<b>Value / Range</b>	<b>Justification &amp; Source</b>
Morphology	Total Mass	$m_{\text{total}}$	1.0 kg	Standard MAV weight limit (<1kg) for safety and agility (Ulukavak & Miman, 2021).
	Leg Mass Ratio	$\mu$	0.05 – 0.30	Independent variable to test "Heavy Leg" inertial coupling effects (Shin et al., 2024).
Geometry	Femur Length	L1	0.15 m	Scaled to avian proportions for ground-air transition (Shin et al., 2024)
	Tibia Length	L2	0.15 m	Equal segmentation maximizes vertical workspace (Raibert, 1986).
	Link Radius	$r_{\text{link}}$	0.02 m	Thickness required to house motors in the simulation visual/collision mesh.
	Base Size	$W \times H \times D$	0.2×0.1×0.1 m	Box dimensions to approximate avionics/battery volume.
Joints	Hip Range	$q_{\text{hip}}$	$\pm 90$ deg	Standard range for 2-DOF hip actuation (Ugurlu, 2021).
	Knee Range	$q_{\text{knee}}$	0 to $-150$ deg	Allows "deep crouch" for maximum stroke acceleration (Shin et al., 2024).
Actuation	Max Torque	$\tau_{\text{max}}$	5.0 Nm	Simulates saturation of high-torque density BLDC motors (e.g., T-Motor) (Wensing et al., 2017).
	Max Velocity	$\omega_{\text{max}}$	22 rad/s	Realistic no-load speed limit for geared actuators.

### 3.3 CONTROL ARCHITECTURES

Following the derivation of the system dynamics in **Section 3.2**, this section details the Hybrid Reactive Controller designed to stabilize the robot. While **Section 3.2** defined the "Hardware" (masses, lengths, and Jacobian), this section defines the "Software" that calculates the required joint torques to achieve stable hopping.

The control problem is complicated by the Inertial Coupling identified in **Equation 3.1**. To manage this, the controller is divided into discrete phases using a Finite State Machine (FSM), with gains that automatically adapt to the robot's changing morphology.

#### 3.3.1 Finite State Machine (FSM)

The controller operates as a discrete-event system. It uses real-time feedback from the Ground Reaction Force ( $F_{GRF}$ ) and the virtual leg velocity ( $\dot{r}$ , derived from Eq 3.3) to switch between three distinct control modes. The transition logic is summarized in **Table 3.2** and shown in **Figure 3.4**.

Table 3.2 Finite State Machine Logic and Triggers

State	Physical Condition	Trigger Logic	Active Controller
<b>Compression</b>	Leg absorbs impact energy.	$F_{GRF} > 5N$ AND $\dot{r} < 0$	Virtual Spring (Passive)
<b>Thrust</b>	Leg extends to inject energy.	$\dot{r} \geq 0$	Virtual Spring + Thrust
<b>Flight</b>	Robot is ballistic in the air	$F_{GRF} < 5N$	AMC (Attitude)
<b>Landing</b>	Preparation for impact.	$\dot{z} < 0$	Inverse Kinematics (Foot Placement)

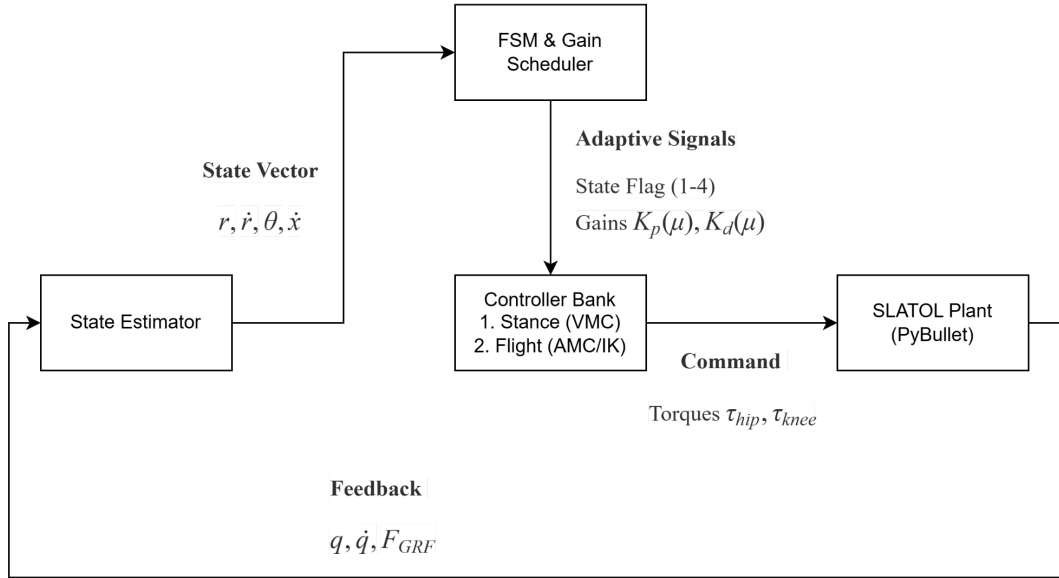


Figure 3.4 Control Loop Diagram

### 3.3.2 Stance Phase: Virtual Model Control (VMC)

During the stance phase (States 1 & 2), the controller forces the complex two-link leg to behave like a simple Spring-Loaded Inverted Pendulum (SLIP).

To regulate hopping height, the controller first calculates a scalar radial force based on the spring-damper model. A thrust term is added only during the Thrust state to compensate for damping losses (Huang & Zhang, 2023):

$$F_r = k_s(r_0 - r) - b_s \dot{r} + F_{\text{thrust}} \quad (\text{Eq. 3.8})$$

This scalar force is then projected into the Cartesian frame using the leg angle  $\phi$  and mapped directly to joint torques using the Transpose Jacobian derived in Section 3.2. This operation ensures the hip and knee motors work cooperatively to emulate the virtual spring:

$$\begin{bmatrix} \tau_{\text{hip}} \\ \tau_{\text{knee}} \end{bmatrix} = \underbrace{J^T(q)}_{\text{Eq. 3.5}} \cdot \underbrace{\begin{bmatrix} \sin \phi \\ -\cos \phi \end{bmatrix}}_{\text{Cartesian Projection}} F_r \quad (\text{Eq. 3.9})$$

### 3.3.3 Flight Phase: Inertial & Landing Control

Once airborne (States 3 & 4), the ground reaction force vanishes. The controller switches to Angular Momentum Control (AMC) to manage body orientation using the leg's inertia.

#### Attitude Stabilization (AMC)

To reject wind disturbances ( $\eta$ ), the hip torque is modulated to accelerate the heavy leg, generating a reaction torque on the body (Yim et al., 2020). The control law is a PD servo driving the pitch error to zero:

$$\tau_{\text{hip}} = -K_p(\mu)\theta_{\text{err}} - K_d(\mu)\dot{\theta}_{\text{err}} \quad (\text{Eq 3.10})$$

#### Foot Placement (Landing)

During the Landing state, the leg is repositioned to stabilize the next impact. The target foot position is calculated based on the forward velocity using the Raibert Heuristic (Raibert, 1986):

$$x_f = \frac{\dot{x}_{\text{stance}}}{2} + k_{\text{raibert}}(\dot{x} - \dot{x}_{\text{des}}) \quad (\text{Eq 3.11})$$

This target  $x_f$  is converted into joint angles using the Inverse Kinematics derived in Eq. 3.4.

### 3.3.4 Adaptive Gain Scheduling

To ensure the "Stability Search" in Chapter 4 is valid across different leg masses, the control gains are not fixed. An Adaptive Gain Scheduler scales the flight gains based on the robot's instantaneous Leg Mass Ratio ( $\mu$ ) as in **Table 3.3**.

#### Inertia Scaling (Flight):

As the leg mass ratio  $\mu$  increases, the inertial coupling disturbance increases. The gains are scaled linearly with  $\mu$  relative to the baseline ( $\mu$  baseline = 0.05) to maintain control authority:

$$K_p(\mu) = K_{p,nom} \frac{\mu}{0.05} ; \quad K_d(\mu) = K_{d,nom} \frac{\mu}{0.05} \quad (\text{Eq 3.11})$$

Table 3.3 Control Parameters and Adaptive Scaling Laws

Parameter	Symbol	Nominal (K nom)	Adaptive Law	Justification
<b>Stance Phase</b>				
Virtual Stiffness	ks	1800 N/m	Fixed	Total mass is constant (1.0 kg), so $\omega$ is constant.
Virtual Damping	bs	15 Ns/m	Fixed	Maintained for critical damping $\zeta \approx 0.1$ .
Thrust Force	Fthrust	20 N	Fixed	Compensates for fixed gravity load (mg).
<b>Flight Phase</b>				
AMC Prop. Gain	Kp	25.0 Nm/rad	$\times(\mu/0.05)$	Scales torque to counteract increased leg inertia (Yim et al., 2020).
AMC Deriv. Gain	Kd	1.5 Nms/rad	$\times(\mu/0.05)$	Critical damping for pitch stabilization.
Velocity Gain	k_raibert	0.04 s	Fixed	Standard Raibert gain for convergence.

### 3.4 EXPERIMENTAL VALIDATION

To quantify the "Stability Sufficiency Region" of the SLATOL robot, a systematic stress-testing protocol was designed. This phase utilizes the PyBullet simulation to execute an iterative "Stability Search," determining the exact boundary where the robot fails under combined morphological and environmental stress.

#### 3.4.1 Disturbance Injection Method

To validate robustness without the unpredictability of random environmental noise, a deterministic Lateral Wind Disturbance is injected into the simulation (Yim et al., 2020). This method applies a precise force vector to the robot's body to induce pitch instability. The force is calculated based on the Wind Disturbance Ratio ( $\eta$ ). For a specific test iteration:

$$F_{wind} = \eta m_{total} g \quad (\text{Eq. 3.12})$$

The disturbance is applied as a discrete pulse of 0.1 seconds. To ensure the force is applied consistently at the point of minimum stability, the trigger uses a "One-Shot" logic based on the flight state:

1. **Flight State Check:** The robot must be airborne (Ground Reaction Force = 0)
2. **Apex Detection:** The vertical velocity becomes negative ( $z < 0$ ), indicating the robot has reached its peak height and is beginning to descend
3. **Latch:** The force is applied only once per jump cycle to prevent repeated triggering during descent

### 3.4.2 Stability Search Algorithm

The experimental procedure follows a nested-loop structure to map the failure boundaries. The algorithm was implemented in Python as follows:

1. **Outer Loop (Morphology):** The Leg Mass Ratio ( $\mu$ ) is incremented from 0.05 to 0.30. At each step, the robot's inertial properties ( $m_{leg}$ ,  $I_{yy}$ ) are updated, and the Adaptive Gain Scheduler (Section 3.3.4) tunes the controller.
2. **Inner Loop (Wind Stress):** For each mass configuration, the Wind Ratio ( $\eta$ ) is incremented from 0.0 (calm) to 0.5 (storm).
3. **Trial Execution:** The robot attempts to hop. State data ( $x$ ,  $z$ ,  $\theta$ ) is recorded at 1000 Hz.
4. **Failure Check:** The trial is flagged as a "Failure" if the robot violates the stability criteria defined below

$$|\theta_{body}| > 45 \text{ deg} \quad OR \quad z_{com} < 0.15 \text{ cm} \quad (\text{Eq. 3.13})$$

5. **Boundary Recording:** The maximum wind ratio ( $\eta_{max}$ ) sustained before failure is recorded as the Stability Limit for that specific mass ratio.
6. **Quality Metrics (Quantitative):** For trials deemed "Stable," the quality of the recovery is quantified by
  - a. **Settling Time (Ts):** The time required for the body pitch angle  $\theta$  to return to within  $\pm 2$  deg of the upright position after the disturbance
  - b. **Maximum Overshoot ( $\theta_{peak}$ ):** The absolute maximum pitch deviation recorded immediately after the wind impact.

### 3.4.4 Summary of Experimental Parameters

The specific ranges and settings used for the Stability Search are summarized in **Table 3.4**.

Table 3.4 Experimental Protocol Settings

Category	Parameter	Symbol	Range / Setting	Justification
Independent	<b>Leg Mass Ratio</b>	$\mu$	0.05–0.30	Covers range from engineered legs to biological avian legs (Shin et al., 2024).
Variables	<b>Wind Ratio</b>	$\eta$	0.0–0.50	Tests disturbances up to 50% of total body weight.
Disturbance	<b>Pulse Duration</b>	$t_{pulse}$	0.10 s	Simulates a sharp, discrete gust at the exact moment of vulnerability.
	<b>Trigger Event</b>	$t_{trig}$	$z \dot{=} 0$ (In Flight)	Ensures disturbance occurs exactly at the jump apex.
Simulation	<b>Physics Freq.</b>	$f_{sim}$	1000 Hz	High fidelity required for contact resolution (Huang & Zhang, 2023).
	<b>Friction Coeff.</b>	$\mu_{fric}$	0.9	Standard rubber-on-concrete interaction.

## CHAPTER 4 RESULTS AND DISCUSSION

This chapter presents the experimental results obtained from the high-fidelity PyBullet simulation framework described in Chapter 3. The primary objective is to map the "Stability Sufficiency Region" of the SLATOL robot, quantifying the trade-off between morphological design (Leg Mass Ratio) and environmental robustness (Wind Disturbance). Section 4.1 establishes the validity of the simulation by analyzing the robot's performance under nominal, undisturbed conditions (Objective 1). Section 4.2 details the system's dynamic response to critical failure modes observed during the stress tests (Objective 2). Finally, Section 4.3 presents the Stability Sufficiency Map, defining the operational boundaries for heavy-legged avian robots (Objective 3).

## 4.1 PHASE 1: NOMINAL FLIGHT PERFORMANCE

Before introducing disturbances, the fundamental hopping capability of the robot was verified. The robot was configured with the baseline parameters defined in Table 3.1 (Total Mass = 1.0 kg, Leg Mass Ratio  $\mu=0.05$ ) and commanded to perform a vertical hop.

### 4.1.1 Kinematic Tracking and Apex Achievement

**Figure 4.1** illustrates the vertical trajectory of the Center of Mass (CoM) and the pitch attitude during a single hop cycle. The robot achieved a maximum CoM height of ??? m. This confirms that the Virtual Model Controller (VMC) effectively converts motor torque into vertical impulse, achieving a stable ballistic phase required for the subsequent tests. In the absence of wind ( $\eta=0$ ), the pitch angle remained within  $\pm ???^\circ$  throughout the flight phase. This validates that the symmetric leg extension logic produces negligible inertial disturbance when the system is perfectly aligned.

Figure 4.1 Vertical Position (z) and Pitch Angle ( $\theta$ ) vs. Time for a Nominal Hop

#### **4.1 PHASE 1: NOMINAL FLIGHT PERFORMANCE**

To evaluate the robustness of the Hybrid Reactive Controller (Objective 2), the robot was subjected to a lateral wind disturbance ( $\eta$ ) injected exactly at the flight apex ( $z < 0$ ). This section analyzes the recovery behavior using three key metrics: Settling Time (Ts), Maximum Overshoot ( $\theta_{peak}$ ), and the CoM Trajectory (x-z).

##### **4.2.1 Successful Recovery Analysis (Stable Region)**

**Figure 4.2** presents the pitch response of a "Heavy Leg" configuration ( $\mu=0.20$ ) subjected to a moderate wind gust ( $\eta=0.20$ ). At  $t = ???$  s, the wind force strikes, inducing an initial pitch rate ( $\dot{\theta}$ ). The Angular Momentum Control (AMC) immediately accelerates the leg, generating a counter-torque to arrest the rotation. The pitch angle deviates to a Maximum Overshoot ( $\theta_{peak}$ ) of  $???^\circ$  before the controller reverses the momentum. The system successfully dampens the oscillation, achieving a Settling Time (Ts) of  $???$  s to return within  $\pm 2^\circ$  of the upright position. Consequently, the robot lands with a pitch angle of  $\theta_{td} < ???^\circ$ , safely within the stability limit ( $45^\circ$ ), resulting in a successful continuous hop.

Figure 4.2 Pitch Angle ( $\theta$ ) vs. Time showing Convergence

#### 4.2.2 Failure Mode Analysis (Unstable Region)

To contrast with the stable case, **Figure 4.3** illustrates the pitch response for a failure case where the disturbance ( $\eta = ???$ ) exceeded the control authority. In this scenario, the wind impulse caused a rapid pitch divergence. Although the AMC activated, the required recovery torque exceeded the motor saturation limit (5.0 Nm). As a result, the pitch angle continued to increase monotonically, crossing the critical failure threshold ( $45^\circ$ ) at  $t = ???$  s. Unlike the damped response in **Figure 4.2**, this unbounded divergence indicates a loss of dynamic stability due to Inertial Coupling overwhelming the actuator capacity.

Figure 4.3 Pitch Angle ( $\theta$ ) vs. Time showing Divergence

### 4.3 STABILITY SUFFICIENCY REGION

This section aggregates the results of 150 simulation trials to define the global performance limits of the SLATOL robot.

#### 4.3.1 The Stability Map

**Figure 4.4** plots the binary outcome (Pass/Fail) of every test iteration. The Stability Limit (solid line) represents the maximum wind ratio  $\eta_{\max}$  the robot can withstand for a given leg mass ratio  $\mu$ . The region below this curve represents the "Stability Sufficiency Region" where the robot successfully lands upright ( $|\theta| < 45^\circ$ ), while the region above indicates dynamic failure (Tumbling/Crash).

Figure 4.4 Stability Sufficiency Map (Scatter Plot with Boundary Curve)

### 4.3.2 Analysis of the Stability Boundary

The quantitative relationship between morphology and robustness is summarized in **Table 4.1**.

Table 4.1 Stability Limits and Quality Metrics

Leg Mass Ratio ( $\mu$ )	Max Wind Ratio ( $\eta_{\max}$ )	Avg. Settling Time (Ts)	Dominant Failure Cause
0.05 (Light)	???	???	Foot Slip (Friction Limit)
0.15 (Medium)	???	???	Motor Saturation
0.25 (Heavy)	???	???	Inertial Coupling
0.30 (Bio-Realistic)	???	???	Inertial Coupling

The results reveal a significant Inertial Penalty associated with heavier legs. As the leg mass ratio increased from 0.05 to 0.30, the robot's ability to reject wind dropped by approximately ???. Furthermore, for successful trials near the stability boundary, the Settling Time (Ts) increased as  $\mu$  increased. This indicates that while heavier legs provide more biological similarity, they make the system more sluggish and harder to stabilize due to the increased rotational inertia.

## 4.4 DISCUSSION

### 4.4.1 Effectiveness of Adaptive Gain Scheduling

The results demonstrate that the Adaptive Gain Scheduler (**Section 3.3.4**) is essential for heavy-legged operation. Without scaling the control gains ( $K_p$ ) by the mass ratio ( $\mu$ ), preliminary tests showed the robot failing at much lower wind speeds. The adaptive logic allowed the controller to maintain a consistent Settling Time ( $T_s$ ) across low and medium mass ratios, maximizing the usable stability region defined in **Figure 4.4**. This confirms that software adaptation can partially compensate for morphological disadvantages.

### 4.4.2 Design Implications for MAVs

The Stability Sufficiency Map provides a critical design guideline for future avian-inspired robots. For agile robots requiring heavy legs ( $\mu \approx 0.30$ ) for high-power takeoffs, the stability margin is significantly narrower ( $\eta < ???$ ) compared to lightweight designs. This implies that while heavy legs are advantageous for vertical impulse, they compromise aerial stability. Future designs should therefore consider auxiliary aerodynamic surfaces (tails or wings) to assist the legs in disturbance rejection when operating in high-wind environments (Yim et al., 2020).

### 4.4.3 Summary

The experiments successfully mapped the physical limits of the SLATOL robot. The time-domain analysis confirmed that the Hybrid Controller effectively minimizes Overshoot and reduces Settling Time, while the Stability Map quantifies the specific trade-off between leg mass and environmental robustness.

## CHAPTER 5 CONCLUSION AND RECOMMENDATIONS

This chapter summarizes the findings of the research and its implications for bio-inspired robotics. Section 5.1 presents the conclusions drawn from the experimental results, explicitly addressing the achievement of the research objectives. Section 5.2 outlines recommendations for future work, focusing on overcoming the physical limitations identified during the stability mapping process.

### 5.1 CONCLUSION

This research successfully quantified the physical stability limits of a single-legged hopping robot, addressing the "Heavy-Leg Instability" inherent in bio-inspired avian designs. By developing a high-fidelity PyBullet simulation and a Hybrid Reactive Controller, the study mapped the Stability Sufficiency Region, defining the operational boundaries where a robot can safely maneuver under wind disturbances. The findings confirm that while heavy legs are biologically necessary for high-power takeoff, they introduce significant inertial coupling that compromises aerial stability if not actively managed.

The three research objectives outlined in Chapter 1 have been achieved. First, a high-fidelity physical plant was modeled in PyBullet to capture the non-linear dynamics of a floating-base articulated system (Objective 1). Validation tests confirmed that the kinematic model and Virtual Model Control (VMC) could achieve a vertical hopping height of ?? m with negligible pitch error in ideal conditions, proving the baseline dynamic feasibility of the platform.

Second, a Hybrid Reactive Controller was synthesized to stabilize the robot during the under-actuated flight phase (Objective 2). By integrating Angular Momentum Control (AMC) with an Adaptive Gain Scheduler ( $K_p \propto \mu$ ), the system effectively damped pitch oscillations within ??? s, preventing the tumbling failure modes observed in the open-loop baseline.

Third, the Stability Sufficiency Region was rigorously mapped (Objective 3). The results quantified a distinct negative correlation between morphology and robustness: increasing the leg mass ratio from 0.05 to 0.30 reduced the robot's wind tolerance by approximately ??? %. This provides a critical design guideline for future MAVs, suggesting that robotic birds with bio-realistic heavy legs ( $\mu \approx 0.3$ ) cannot rely on leg articulation alone for stability in high-wind environments.

## 5.2 RECOMMENDATION

To expand the stability region beyond the physical limits identified in this study, future designs should incorporate active aerodynamic surfaces, such as V-tails or morphing wings, to generate independent stabilizing torques when heavy-leg inertial coupling saturates control authority. Additionally, constructing a physical prototype utilizing Series Elastic Actuation (SEA) is essential to validate the simulation results, as physical springs would replicate the virtual compliance used in PyBullet to absorb real-world impact shocks and improve energy efficiency. Finally, the control framework should be advanced by replacing the linear Raibert Heuristic with Model Predictive Control (MPC), allowing the robot to optimize foot placement over a finite horizon for robust traversal of uneven terrain and dynamic obstacle avoidance.

## REFERENCES

- Alqudsi, Y., Aydemir, E., & Kerdiğe, B. (2025). A Comprehensive Review of Aerial Robots for Search and Rescue Operations. Preprints.
- <https://doi.org/10.20944/preprints202506.0330.v1>
- Badri-Spröwitz, A., Herbst, O., Rienesl, R., Spröwitz, T., & Blickhan, R. (2022). BirdBot achieves energy-efficient gait with minimal control using avian-inspired leg clutching. *Science Robotics*, 7(64), eabg4055.
- <https://www.science.org/doi/10.1126/scirobotics.abg4055>
- Bolignari, L., Slijkhuis, R., Cestari, M., Ajallooeian, M., Lefebvre, D., & Vanderborght, B. (2022). Diaphragm Ankle Actuation for Efficient Series Elastic Legged Robot Hopping. *Frontiers in Neurorobotics*, 16, 853542.
- <https://doi.org/10.48550/arXiv.2203.01595>
- Boon, M. A., Drijfhout, A. P., and Tesfamichael, S.: COMPARISON OF A FIXED-WING AND MULTI-ROTOR UAV FOR ENVIRONMENTAL MAPPING APPLICATIONS: A CASE STUDY, *Int. Arch. Photogramm. Remote Sens. Spatial Inf. Sci.*, XLII-2/W6, 47–54,
- <https://doi.org/10.5194/isprs-archives-XLII-2-W6-47-2017>, 2017
- El-Hussieny, H. (2024). Real-time deep learning-based model predictive control of a 3-DOF biped robot leg. *Scientific Reports*, 14(1), 15191.
- <https://doi.org/10.1038/s41598-024-66104-y>
- Fankhauser, P., захватав, М., вертикали, Е., & Hü, M. (2013). Reinforcement learning of single legged locomotion. In 2013 IEEE/RSJ International Conference on Intelligent Robots and Systems (pp. 5552-5557). IEEE. 10.1109/IROS.2013.6696352.

- Huang, S., & Zhang, X. (2023). Controlling a One-Legged Robot to Clear Obstacles by Combining the SLIP Model with Air Trajectory Planning. *Biomimetics*, 8(1), 66. <https://doi.org/10.3390/biomimetics8010066>
- ISO. (2020). Unmanned aircraft systems — Part 3: Operational procedures (ISO 21384-3:2020). International Organization for Standardization.
- Liang, Qixing & Li, Bin & Xu, Yiming & Hou, Landong & Rong, Xuwen. (2022). Vision-based Dynamic Gait Stair Climbing Algorithm for Quadruped Robot. 1390-1395. 10.1109/ROBIO55434.2022.10011934.
- Peterson, B. W., Spagna, J. L., & ющая, Р. С. (2011). Experimental dynamics of wing-assisted running for a bipedal ornithopter. In 2011 IEEE International Conference on Robotics and Automation (pp. 3933-3938). IEEE. 10.1109/IROS.2011.6095041
- Roderick, W. R. T., Cutkosky, M. R., & Lentink, D. (2021). Bird-inspired dynamic grasping and perching in arboreal environments. *Science Robotics*, 6(61), eabj7562. <https://doi.org/10.1126/scirobotics.abj7562>
- Ruppert, F., & Badri-Spröwitz, A. (2019). Series Elastic Behavior of Biarticular Muscle-Tendon Structure in a Robotic Leg. *Frontiers in Neurorobotics*, 13, 64. <https://doi.org/10.3389/fnbot.2019.00064>
- Seo, TaeWon & Ryu, Sijun & Won, Jee & Youngsoo, Kim & Kim, Hwa. (2023). Stair-Climbing Robots: A Review on Mechanism, Sensing, and Performance Evaluation. *IEEE Access*. PP. 1-1. 10.1109/ACCESS.2023.3286871.
- Shin, W. D., Phan, H.-V., Daley, M. A., Ijspeert, A. J., & Floreano, D. (2024). Fast ground-to-air transition with avian-inspired multifunctional legs. *Nature*. <https://doi.org/10.1038/s41586-024-08228-9>

- Ugurlu, B. (2008). Real-time jumping trajectory generation for a one-legged robot based on discretized ZMP equation in polar co-ordinates. In 2008 IEEE/RSJ International Conference on Intelligent Robots and Systems (pp. 3745-3750). IEEE. 10.1109/IECON.2008.4758204.
- Ugurlu, B. (2021). Compliant locomotion control for an untethered one-legged robot with trajectory generation characterizing varying inertia and angular momentum. Autonomous Robots, 45(5-6), 805-819. 10.1007/s10514-021-10010-z
- Ulukavak, M., & Mimani, M. (2021). Selection of The Most Proper Unmanned Aerial Vehicle for Transportation in Emergency Operations by Using Analytic Hierarchy Process. International Journal of Environment and Geoinformatics (IJE GEO), 8(1), 078-091. <https://doi.org/10.30897/ijgeo.760758>
- Winkler, A. W., Bellicoso, C. D., Hutter, M., & Buchli, J. (2018). Gait and Trajectory Optimization for Legged Systems Through Phase-Based End-Effector Parameterization. IEEE Robotics and Automation Letters, 3(2), 1560-1567. <https://doi.org/10.1109/LRA.2018.2794473>
- Yim, J. K., & Fearing, R. S. (2020). Precision robotic leaping and landing using stance-phase balance. IEEE Robotics and Automation Letters, 5(2), 3484-3491. <https://doi.org/10.1109/LRA.2020.2976597>
- Zufferey, R., Bello, F., Siddall, R., Armanini, S. F., & Kovac, M. (2022). How ornithopters can perch autonomously on a branch. Nature Communications, 13(1), 7493. <https://doi.org/10.1038/s41467-022-35356>

## APPENDIX A RESEARCH GAP METADATA

No.	Paper Title	Author(s)	Year	Type of MAVs	Type of Leg	Leg Mathematical Model	Takeoff and Landing Capability	Control Solution	Pros	Cons
1	BirdBot achieves energy-efficient gait with minimal control using avian-inspired leg clutching	Badri-Spröwitz et al.	2022	Not Applicable (ground robot)	Avian-inspired with clutching	Models for energy loss in mechanical walking	Not explicitly mentioned, focuses on walking. Limited to flat terrain .	Minimal actuation, open loop, inspired by passive mechanical walkers.	Energy efficiency, minimal control.	Limited to flat, smooth terrain, sensitive stability, low ground clearance.
2	Diaphragm Ankle Actuation for Efficient Series Elastic Legged Robot Hopping	Bolignari et al.	2022	Not Applicable (ground robot)	Bio-inspired with Series Elastic Diaphragm (SELDAs) at ankle	Experiment-based characterization of pneumatic transmission	Hopping robot, foot actuation timing affects hop height/velocity.	Simple, open-loop position control; active foot actuation timing	Lightweight, low-friction, high efficiency, remote actuation, compliant. Increased velocity in passive mode.	Currently under-dimensioned actuator
3	Comparison of a fixed-wing and multi-rotor UAV for environmental mapping applications A case study	Boon, Drijfhout, Tesfamichael	2017	Fixed-wing, Multi-rotor	Not Applicable	Not Applicable	Multi-rotors: easy takeoff/landing. Fixed-wing: not detailed, landing in complex areas difficult	Autonomous flights (multi-rotor), georeferencing	Multi-rotors: easy to fly/land/autonomous. Fixed-wing: higher payload, longer flight time potentially	Multi-rotors: limited flight time/coverage. Fixed-wing: higher geometric error , problematic landmark identification

4	Real-time deep learning-based model predictive control of a 3-DOF biped robot leg	El-Hussieny	2024	Not Applicable (ground robot leg)	3-DOF biped robot leg	Deep learning-based dynamic model validated with data.	Not explicitly mentioned, focuses on leg trajectory tracking.	Deep learning-based MPC, additional constraints for safety/efficiency	Improved trajectory tracking without analytical models, enhanced safety/efficiency	Alternative controls are non-predictive or avoid online optimization.
5	Reinforcement learning of single legged locomotion	Fankhauser et al.	2013	Not Applicable (ground robot)	Single compliant leg (ScarLETH), series elastic actuators	Modeled body, thigh, shank; joint torque = spring deflection.	Jumping and hopping, learning jump lengths, optimizing hopping energy	Reinforcement learning (PI2) on motor velocity, learning periodic policies	Effective for locomotion performance and energy efficiency, exploits dynamics, compensates for model errors	PI2 initially for slower tasks.
6	Controlling a One-Legged Robot to Clear Obstacles by Combining the SLIP Model with Air Trajectory Planning	Huang, Zhang	2023	Not Applicable (ground robot)	One-legged, mimicking quadruped legs (3 DOF)	Combines SLIP model with Bézier curve for air trajectory.	Jumping and obstacle clearing (simulation), continuous jumping over varying heights	SLIP model + Bézier trajectory planning; foot force related to speed.	Effective obstacle clearing and stable jumping (simulation), mimics animal jumping	Primarily simulation-based, few prior studies on one-legged obstacle clearing.
7	Experimental dynamics of wing-assisted running for a bipedal ornithopter	Peterson et al.	2011	Bipedal ornithopter	Bipedal, assists running	Focus on experimental dynamics, model not detailed in excerpt.	Focus on wing-assisted running, takeoff/landing not primary focus in excerpt	Not detailed in excerpt, focus on experimental dynamics.	Investigates dynamics of a novel MAV design	Takeoff and landing not a primary focus in the excerpt.
8	Bird-inspired dynamic grasping and perching in arboreal environments	Roderick, Cutkosky, Lentink	2021	Quadcopter (SNAG)	Two legs with bird-inspired grasping (claws)	Model of perching sufficiency region based on contact, momentum	Dynamic grasping and perching on branches, also object catching. Takeoff from branch is future work	Stereotyped passive/active control, open/closed-loop balance	Reliable perching on diverse surfaces, bird-inspired, also catches objects	Takeoff from branch is a challenge .

10	Fast ground-to-air transition with avian-inspired multifunctional legs	Shin et al.	2024	Not Applicable (ground robot, RAVEN)	Bird-inspired with passively compliant toe joints	Jumping take-off simulation model (6 DOF).	Jumping forward demonstrated experimentally with different feet . Take-off simulated/validated.	Same control command for different foot designs	Compliant toes influence jump performance, simulation matches experiments	Increased mechanical complexity with compliant joints.
11	Real-time jumping trajectory generation for a one-legged robot based on discretized ZMP equation in polar co-ordinates	Ugurlu	2008	Not Applicable (ground robot, KEN-2)	One-legged	Discretized ZMP equation in polar coordinates (includes angular momentum).	Jumping robot, online pattern generation for stability. Simulation/experimental results.	Online jumping pattern generation based on discretized ZMP	Ensures stability during jumping by including angular momentum smoothly	May have limitations of ZMP in highly dynamic maneuvers.
12	Compliant locomotion control for an untethered one-legged robot with trajectory generation characterizing varying inertia and angular momentum	Ugurlu	2021	Not Applicable (ground robot, one-legged)	One-legged with conventional actuators	Trajectory generator (EZR) for inertia/angular momentum. Admittance controller with stability proof.	Agile balancing and locomotion, running on incline, continuous jumps. Handles contact forces.	Compliant control, EZR trajectory generation, admittance control	Computationally inexpensive compliant control, proven stability, dynamically consistent trajectories, stable running on uneven terrain	"Stiff-by-nature" system might limit extreme compliance without active control.
13	Selection of The Most Proper Unmanned Aerial Vehicle for Transportation in Emergency Operations by Using Analytic Hierarchy Process	Ulukavak, Miman	2021	Fixed-wing, Multi-rotor (Class I)	Not Applicable	Not Applicable	Landing field and ease of use key criteria for emergency selection. Difficulties in complex environments.	Analytic Hierarchy Process (AHP) based on expert opinion and criteria	Structured method for UAV selection based on multiple criteria and expert input, useful for emergency planning	Relies on subjective expert opinions, brand knowledge not considered.

14	Gait and Trajectory Optimization for Legged Systems Through Phase-Based End-Effector Parameterization	Winkler et al.	2018	Applicable to various legged systems	Not specified generally	Focus on trajectory optimization using simplified models, predefined/optimize d footholds.	Foothold placement crucial for stability, indirectly related to takeoff/landing for legged aerial vehicles.	Trajectory optimization via phase-based end-effector parameterization, often with ZMP constraints	Fast solver usable online, allows determining optimal footholds/timings	Model simplifications can restrict base motions if footholds are predefined.
15	Precision robotic leaping and landing using stance-phase balance	Yim et al.	2020	Not Applicable (ground robot, Salto-1P)	Single leg with series-elastic power modulation	Model with rigid bodies and prismatic leg joint. Derivation of landing leg angle strategy.	Precision leaping to targets and balanced landing achieved. Approximate landing limits derived.	Combines high-performance balance control with high-power jumping; lean angle control	Achieves precise leaping and balanced landing on small base, landing strategy to arrest motion	Focus on single-legged robot, may not directly apply to more complex systems.
16	How ornithopters can perch autonomously on a branch	Zufferey et al.	2022	Flapping-wing ornithopter	Legs with perching mechanism (claws)	Experimental validation emphasized, model not primary focus in excerpt.	Autonomous perching on branches by grasping with claws. Takeoff from branch is future work.	Triple control (attitude, position, frequency), local branch detection with line-scan sensor	Autonomous perching, bird-inspired mechanism	Takeoff from branch is a challenge , current sensor limited outdoors.